Programming hydrogel adhesion with engineered polymer network topology

Zhen Yang $^{\rm a}$, Guangyu Bao $^{\rm a,2}$, Ran Huo $^{\rm a,2}$, Shuaibing Jiang $^{\rm a}$, Xingwei Yang $^{\rm b}$, Xiang Ni $^{\rm a}$, Luc Mongeau $^{\rm a,c}$, Rong Long $^{\rm b}$, and Jianyu Li $^{\rm a,c,1}$

^aMechanical Engineering, McGill University, Montreal, H3A 0C3, QC, Canada.; ^bMechanical Engineering, Colorado University Boulder, Boulder, 80309, CO, USA.; ^cBiomedical Engineering, McGill University, Montreal, H3A 2B4, QC, Canada.

This manuscript was compiled on July 31, 2023

10

11

12

13

17

11

12

Hydrogel adhesion that can be easily modulated in magnitude, space, and time is desirable in many emerging applications ranging from tissue engineering and soft robotics to wearable devices. In synthetic materials, these complex adhesion behaviors are often achieved individually with mechanisms and apparatus that are difficult to integrate. Here, we report a universal strategy to embody multifaceted adhesion programmability in synthetic hydrogels. By designing the surface network topology of a hydrogel, supramolecular linkages that result in contrasting adhesion behaviors are formed on the hydrogel interface. The incorporation of different topological linkages leads to dynamically tunable adhesion with high-resolution spatial programmability without alteration of bulk mechanics and chemistry. Further, the association of linkages enables stable and tunable adhesion kinetics that can be tailored to suit different applications. We rationalize the physics of polymer chain slippage, rupture, and diffusion at play in the emergence of the programmable behaviors. With the understanding, we design and fabricate various soft devices such as smart wound patches, fluidic channels, drug-eluting devices, and reconfigurable soft robotics. Our study presents a simple and robust platform in which adhesion controllability in multiple aspects can be easily integrated into a single design of a hydrogel network.

polymer gels | hydrogel adhesives | controlled adhesion | polymer entanglement

he precise programming of hydrogel adhesion, including its magnitude, kinetics, and spatial distribution, has significant implications for engineering, biology, and medicine. The ability to control adhesion energy is essential for bonding reinforcement or easy detachment after placement (1-3), while the ability to control adhesion spatially is useful for applications requiring varying adhesion properties on the targeted surface such as wound dressings (4). While most current research has focused on the adhesion magnitude at the equilibrium stage, controlling adhesion kinetics, which involves modulating transient adhesion over time, is less explored but equally important as it allows for tuning the operating time window for adhesive placement. As such, programming the multifaceted nature of hydrogel adhesion could enable and improve various applications ranging from tissue repair to soft robotics. However, such programmable adhesion is difficult to achieve for synthetic adhesives because they require the addition of complex chemistry and apparatus that are potentially difficult to integrate. For instance, tough hydrogels with covalent bond-based adhesion provide robust adhesion to diverse surfaces (5), but it is challenging to modulate their adhesion without introducing specific chemistry (6). In contrast, physical interactions offer more flexibility to modulate hydrogel adhesion energy, but they require specific material properties (e.g., viscoelasticity) or additional apparatus (light,

ultrasound, etc.) (7–9). In terms of controlling adhesion kinetics, the rate of covalent bonding is fundamentally limited by the specific chemical reactions involved. Physical interactions such as hydrogen bond often form instantaneously (10), providing limited tunability in terms of adhesion kinetics. Achieving spatial control of adhesion requires sophisticated patterning and treatment of the opposing surface (11, 12), and the outcome could be compromised by uncontrolled diffusion of chemical reagents, especially when the two adherends are sufficiently permeable (7). Selective masking of the opposing surface could enable spatially controlled adhesion (13–15), but may be difficult to perform on highly-uncontrolled and unpredictable surfaces such as biological tissues. A universal design strategy that inherently allows for robust and multifaceted adhesion programming on diverse surfaces is still missing.

28

29

30

31

32

33

35

36

37

38

39

40

41

42

43

45

46

47

It has been found that cells utilize dynamic bonding through non-covalent protein-protein interactions, known as slip bonds (16, 17). These bonds exhibit dynamic adhesion strength, with a shorter lifetime under applied force due to the reduced energy barrier to bond rupture, allowing them to switch between bonding and motile states under different physiological environments (18). Furthermore, cells can achieve complex spatiotemporal adhesion controls (19, 20), which are not yet seen among synthetic hydrogel adhesives. In this study, we present a novel approach to engineer surface network topology in hydrogels, which enables the creation of polymer entanglement referred to as the slip linkage (Fig 1a). The slip linkage

Significance Statement

Programming hydrogel adhesion in multiple aspects including adhesion energy, kinetics, and spatial distribution can enable and improve various applications in engineering and medicine yet remains challenging in synthetic hydrogel adhesives. Existing paradigms rely on the addition of chemistries, function materials, or external apparatus, so that the complexity and incompatibility among different components complicate the adhesion programming. Here we present that engineering the surface network topology of a hydrogel adhesive enables embodied programmable adhesion, including controllable adhesion energy, kinetics, and spatial distribution. The robust and versatile strategy works for highly uncontrolled targeted substrate such as biological tissues, and enables the design of numerous soft devices such as a selective wound patch.

The authors declare no competing financial interests.

 $^{^{2}\ \}mathrm{Guangyu}\ \mathrm{Bao}\ \mathrm{contributed}\ \mathrm{equally}\ \mathrm{to}\ \mathrm{this}\ \mathrm{work}\ \mathrm{with}\ \mathrm{Ran}\ \mathrm{Huo}.$

¹To whom correspondence should be addressed. E-mail: jianyu.li@mcgill.ca

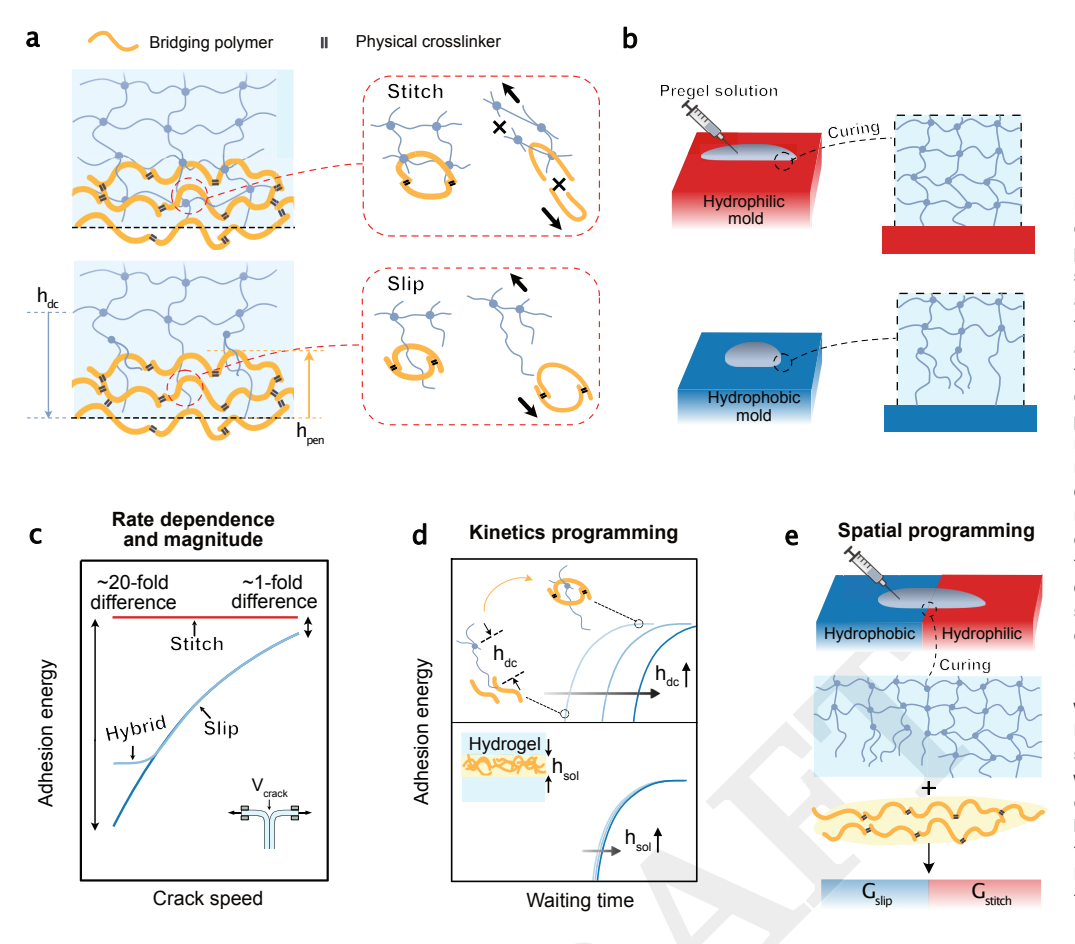


Fig. 1. Engineered network topology and linkages for multifaceted programming of hydrogel adhesion. (a) Schematics of the stitch linkage (Top) and slip linkage (Bottom) formed between a bridging polymer and networks without and with surface dangling chains. The thickness of the dangling chain layer and the penetration depth of the bridging polymer are denoted as $h_{
m dc}$ and $h_{
m pen}$, respectively. (b) Hydrophilic and hydrophobic molds are used to form a regular network (Top) and a network carrying surface dangling chains (Bottom), respectively. (c) Rate dependence and magnitude of the adhesion energy depend on the interfacial linkage types: stitch linkages with $h_{\mathrm{pen}}/h_{\mathrm{dc}}
ightarrow \infty$, slip linkages with $h_{
m pen}/h_{
m dc}~\ll~1$, and their hybrid with $h_{
m pen}/h_{
m dc}~pprox~1.$ (d) The slip linkage offers programmable adhesion kinetics through tuning $h_{\rm dc}$ (Top), which is also insensitive to processing conditions such as the thickness of bridging polymer solution $h_{
m sol}$ (Bottom). (e) Spatially controllable adhesion obtained from patterning the topological linkages at the interface.

81

82

83

86

87

88

89

90

91

93

94

95

96

97

98

99

101

102

103

104

105

106

107

has a topology of a long polymer chain entangled with another crosslinked network (chain-to-network) and can dissociate via chain slippage, a thermally activated process that results in dynamic adhesion analogous to slip bonds in cell adhesion. This enables the adhesion energy to be varied by many folds without background dissipation (Fig 1c). Moreover, the kinetics of slip linkage association dominates over other sub-kinetics that are dependent on operating conditions. By carefully tuning the governing length scale, it is possible to control the kinetics of slip linkage association, resulting in a stable adhesion kinetics with adjustable half time ranging from ~ 50 s to ~ 1000 s (Fig 1d). Furthermore, we demonstrate a simple fabrication method to pattern the slip linkage with another type of polymer entanglement, the stitch linkage, at the same interface (Fig 1b,e). The stitch linkage has the topology of two crosslinked polymer networks entangled together (network-tonetwork), as found in the hydrogel topological adhesion and offers less tunability in terms of adhesion energy and kinetics (7). These two entanglement types display contrasting adhesion behaviors, allowing for pre-definable and spatially-varying adhesion on diverse surfaces. Thus, our study provides an approach to embody multifaceted adhesion programmability into a hydrogel adhesive through a single design of the network structure. We refer to this approach as the topologically engineered adhesives (TEA), which offers a robust, facile, and predictive strategy for unprecedented control over hydrogel adhesion, and opens up numerous opportunities in engineering and medicine.

Results and Discussion

To robustly program hydrogel adhesion, we create a diffusive interface by placing a third species of diffusive polymer, called bridging polymer, to the interface between hydrogel adhesives and targeted surfaces(7, 21). Formation of the chain-to-network topology of the slip linkage demands the following conditions: (1) the hydrogel network needs to contain dangling chains and (2) a thermodynamic driving force is needed to facilitate the diffusion of bridging polymers into the gel network. Meanwhile, the diffusion needs to be halted once the linkage forms to prevent the over-diffusion of bridging polymers into the bulk gel, which may reduce the number of linkages at the interface.

To meet the first condition, we choose polyacrylamide (PAAm) as a model hydrogel network and polymerize it on a mold with low surface tension such as Poly(methyl methacrylate) (PMMA). The hydrophobicity and other associated effects inhibit the free-radical polymerization of the gel in the vicinity of the mold (22–24). This effect results in a surface layer of branched dangling chains with thickness $h_{\rm dc}$ ranging from ~ 10 to $\sim 100~\mu m$ estimated using our experimental results (described later), "protruding" from the crosslinked bulk network. This estimation is in reasonable agreement with an early study (23) showing that a layer of much lower polymer content forms near the surface of Teflon mold during the polymerization of poly-2-acrylamide2-methyl-1-propanesulfonic acid (PAMSP) and poly-acrylic acid (PAAc). The low polymer content layer has a thickness spanning over $\sim 100 \mu m$, which manifests as a dangling chain layer when the gel fully cures. In

54

55

57

58

59

60

61

62

63

64

65

66

67

68

71

72

73

74

75

77

78

79

ຂດ

contrast, gels polymerized on molds with high surface tension such as glass are not subject to the hydrophobic mold effect, and hence contain crosslinked networks instead of branched dangling chains on their surfaces. The gels with and without engineered surface dangling chains are hereafter referred to as the TEA and regular gels, respectively. To meet the second criterion, stimuli-responsive polymers such as chitosan or gelatin were chosen as bridging polymers. The polarity of the hydrogel network and chitosan chains and the entropy of mixing promote the diffusion of chitosan chains into the hydrogel; meanwhile, the chitosan chains can be triggered to crosslink into a bridging network through a reaction-diffusion process in responding to pH changes, leading to penetration depths $h_{\rm pen}$ on the order of tens of microns (21). Other strategies to form the chain-to-network topology of slip linkage at soft material interfaces are discussed in SI Appendix note 1.

110

111

112

113

114

115

116

117

118

119

120

123

124

125

126

127

128

129

130

131

132

133

134

135

136

137

139

140

141

142

143

144

145

146

148

149

150

151

152

153

156

157

158

159

160

161

162

163

164

165

166

167

168

170

Structural characterization. Based on the above principles, we fabricate a model TEA using single-network TEA gel made of PAAm and use chitosan as the bridging polymer. To probe the engagement length between the dangling chains and the bridging polymer chains, we used confocal microscopy to visualize how fluorescently labelled chitosan chains penetrate the TEA gel at equilibrium. The fluorescence intensities exponentially decrease from the outermost surface to the bulk of the TEA gels with different crosslinker-to-monomer ratios C (colored dash lines, Fig 2a). For different C, we measured similar distances where the intensities meet the lower plateau (black dash line, Fig 2a), defining the penetration depth of the bridging polymer $h_{\rm pen} \approx 70 \mu m$. Note that $h_{\rm pen}$ may depend on the polydispersity of chitosan polymers (SI Appendix Fig S9). A systematic study with carefully controlled chitosan polymer molecular weight and C varied in a wide range is needed for a holistic investigation on the relation between the $h_{\rm pen}$ and C. Further, this value may also depends on the reaction-diffusion process and thus may vary with the type of bridging polymers. For instance, $h_{\rm pen}$ for gelatin is expected to be temperature-dependent.

To confirm the presence of the dangling chain layer in TEA gels, we utilized scanning electron microscopy (SEM) to examine a cryosectioned and dehydrated TEA gel sheet (100 μ m thick, SI Appendix note 1 and Fig S3). The dehydrated TEA gel sheet exhibited more pronounced edge shrinkage compared to a regular gel sheet. This phenomenon is presumably due to the lower polymer content and crosslinking density near the edge then in the bulk, indicating the presence of the dangling chain layer near the surface of TEA gels. Since directly imaging the dangling chains is challenging, we made a first-order estimation of the thickness $h_{\rm dc}$ of the dangling chain layer from the experimentally measured elastic moduli. The TEA gel has a total thickness of h and is idealized with a tri-layer model (Fig 2b): a layer of a regular network is sandwiched by two layers of branched dangling chains. The elastic modulus of the sandwiched regular network E_{reg} can be measured from a regular hydrogel formed at the same conditions except using a hydrophilic mold, given their observed structural similarity (23–25). The elastic modulus of the dangling chain layer is assumed to be negligible since it cannot carry any transverse loads. As such, we can estimate $h_{\rm dc}$ from the ratio of measured elastic moduli of the TEA and regular gels $E_{\rm tea}/E_{\rm reg}$ in uniaxial tensile tests (Fig 2c, SI Appendix note 1 and Fig. S1). We further perform micro-indentation test to ascertain the dangling chain layer thickness, and the results show reasonable agreement with the $h_{\rm dc}$ estimation from uniaxial tensile test if considering the non-zero compressible modulus of the branched dangling chains (SI Appendix note 1). The estimations of $h_{\rm dc}$ show a decreasing trend with the increasing value of C. The trend $h_{\rm dc} \sim C^{-1}$ may be attributed to the competition between bulk elasticity of the gel network and interface tension during gelation on hydrophobic mold(22) (SI Appendix note 1), demonstrating a controlled method for fabricating the dangling chain layer of different sizes.

171

172

173

174

175

177

178

179

180

181

182

184

185

186

187

188

189

191

192

193

194

195

196

197

199

200

201

202

203

204

205

206

207

208

209

210

211

212

213

214

216

217

218

219

220

221

222

224

225

226

227

228

229

230

With the measured length scales, we calculate their ratio $h_{\rm pen}/h_{\rm dc}$ to quantify the extent to which the bridging polymers engage the dangling chains, which is expected to govern the formation of different topological linkages at the TEA gel interface (SI Appendix Fig. S4a). When $h_{\rm pen}/h_{\rm dc} \ll 1$, the bridging network only engages a part of the dangling chain layer, so that the interface only comprises slip linkage. If $h_{\rm pen}/h_{\rm dc}\approx 1$, a complete engagement ensues which indicates that part of the bridging polymers may diffuse across the dangling chain layer to stitch the underlying network of the TEA gel. In this case, the linkage is expected to behave as the combination of the slip and stitch linkage and is referred to as the hybrid linkage (Fig 1c). Lastly, a regular hydrogel interface that only comprises stitch linkage corresponds to $h_{\rm pen}/h_{\rm dc} \to \infty$ since $h_{\rm dc} \to 0$. Fig 2c shows $h_{\rm pen}/h_{\rm dc} \approx 0.2$ when C = 0.024% and increases to unity as C increases to 0.06% for the TEA gel interface. By tuning C, we can vary the degree of engagement and consequently the formation of different linkages, which will be shown later to modulate the resulting adhesion energy.

Interfaical topological linkages to program rate-dependent adhesion energy. To test our hypothesis, we first focus on two extremities: the interfaces containing either slip or stitch linkages. To form slip linkage-mediated adhesion, we adhere two TEA gels using chitosan as the bridging polymer with $h_{\rm pen}/h_{\rm dc} \approx 0.2$ (C = 0.024%), followed by a T-peeling specimen to measure the adhesion energy G as a function of crack speed V_{crack} (Methods). Fig 2d shows that the slip linkagemediated adhesion $G^{1/2}$ varies logarithmically with $V_{\rm crack}$, the crack speed. We observed a factor of 25 in the change of Gas $V_{\rm crack}$ varies by two decades. Together plotted in Fig 2d is the stitch linkage-mediated adhesion formed between two regular hydrogels for the same C and chitosan concentration c_{chi} , showing higher magnitude but much weaker rate-dependence. The contrast between slip and stitch adhesion is the most pronounced at low V_{crack} but diminishes at high V_{crack} . We also observed adhesive failure and mixed adhesive-cohesive failure at the slip and stitch linkage-mediated interfaces, repspectively. Our experiments further confirmed the similar bulk mechanics between the TEA and the regular gels: they both show minimal hysteresis in cyclic loadings and weak rate dependences, indicating near-perfect elasticity (SI Appendix Fig. S1a-b). The data suggest that different interfacial network topologies regulate hydrogel adhesion independent of the bulk properties.

These results motivate us to further analyze the data with a kinetic model proposed by Chaudhary (26). The model considers the breaking of linkages as thermally activated processes (26–29), and treats each linkage as a linear spring with stiffness k_i and an activation energy of dissociation E_i (i can be slip or stitch). These parameters influence the dissociation rates of

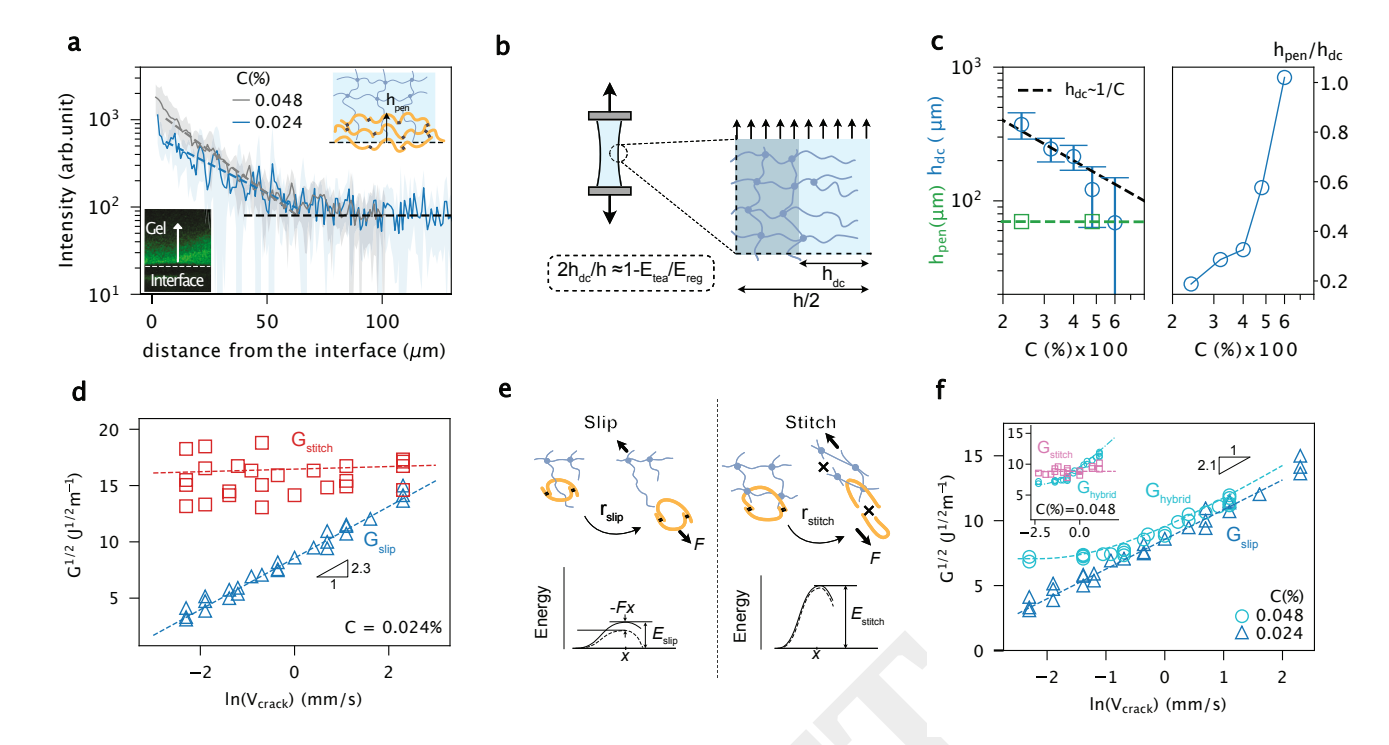


Fig. 2. Design and characterization of topology-engineered adhesive (TEA). (a) Intensities of florescent chitosan chains diffused in TEA gels. The shaded area represents the standard deviation from 5 measures. The stronger chitosan intensity for higher C may be due to more chitosan chains trapped by the denser dangling chains on the interface. (b) An idealized model used to estimate the thickness of branched dangling chain layer. (c) Left panel: estimated $h_{\rm dc}$ and measured $h_{\rm pen}$ as functions of the crosslinker-to-monomer ratio C. Error bars represent standard deviation. Right panel: relative engagement length $h_{\rm pen}/h_{\rm dc}$ as a function of C. Dissimilar topological linkages lead to contrasting adhesion behaviors. (d) Slip and stitch linkages-mediated $G^{1/2}$ plotted as functions of $\ln(V_{\rm crack})$ for C=0.024% and $c_{chi}=2\%$ g/mL. (e) Illustration showing the dissociations of slip and stitch linkages as thermally activated processes, with reaction rate of dissociation r_i (i can be slip or stitch). Upon a separation force F, the activation energy of the linkage is decreased by -Fx, where x is the separation distance. (f) The formation of topological linkages and the resulting adhesion depend on $h_{\rm pen}/h_{\rm dc}$, which is controlled by C. Slip and hybrid linkages are achieved for TEA gels with C=0.024% and 0.048%, respectively. The inset shows the same curves as (d) but for C=0.048%.

the linkages (Fig 2e), and consequently the rate-dependence of the hydrogel adhesion energy. As detailed in SI Appendix note 2, the model states the adhesion energy for linkage i relates to the crack speed via $G^{1/2} \sim \ln V_{\rm crack}$, which agrees perfectly with our experimental data for the slip linkage-mediated adhesion (blue dash lines in Fig 2d). Further, the model shows that the slope of the linear relation scales inversely to $k_i^{1/2}$, while the intercept depends on E_i . By fitting this model to our data we were able to determine k_i and E_i , which are otherwise difficult to characterize directly. Specifically, we found $k_{\rm slip} = 1.7 \times 10^{-7}$ N/m and $E_{\rm slip} = 75$ kJ/mole for the slip linkage with C = 0.024% and $h_{\rm pen}/h_{\rm dc} \approx 0.2$. It is plausible that the hydrogel dangling chains that determine $k_{\rm slip}$ is of entropic type, so that $k_{\rm slip} = 3k_BT/R^2$ with k_BT the energy in temperature and R the average end-to-end distance of the dangling chains. The model allows us to estimate $R\approx 250~\mathrm{nm}$ with the fitted value of $k_{\rm slip}$, which is 50 times larger than the mesh size of the underlying network $\xi \approx 5$ nm (SI Appendix note 1). The fitted value of $E_{\rm slip}$ is larger than the typical activation energy of hydrogen bond (4-50 kJ/mole), suggesting potential synergistic contributions of multiple hydrogen bonds (between chitosan and PAAm) to a single slip linkage. Besides, the model captures the rate-insensitivity of $G_{\rm stitch}^{1/2}$ of the stitch linkage with $k_{\rm stitch} \gtrsim 300 k_{\rm slip}$ and $E_{\rm stitch} \approx 185$ kJ/mole (red dash line, Fig 2d). The much larger k_{stitch} may be due to the full extension of the entangled networks prior to network rupture, driving the polymer chains far beyond the entropic

limit. The estimation of $E_{\rm stitch}$ is in the range of the bond energy of the C-C bond (350 kJ/mole) (30) and the theoretically estimated energy stored in each bond prior to rupture using molecular parameters (60 kJ/mole)(31), in line with the assumption that the stitched networks must rupture during separation. This model reveals quantitatively that the slip linkages exhibit much lower stiffness and dissociation energy compared to those of stitch linkages.

Additionally, the model predicts that the hybrid linkage formed when $h_{\rm pen}/h_{\rm dc}$ is close to 1, would impart tunable dependence on loading rate through the relation $G_{\text{hybrid}} =$ $G_{\text{slip}} + G_{\text{stitch}}$. In this case, $G_{\text{hybrid}}^{1/2}$ is predicted to be a nonlinear function of $\ln V_{\rm crack}$ with a finite and constant value of G_{stitch} (Fig 1c), indicating that the hybrid linkage behaves as slip or stitch linkage respectively in different ranges of loading rates. To test the hypothesis, we prepared TEA gels with $h_{\rm pen}/h_{\rm dc}\approx 0.6$ (C = 0.048%, Fig 2c), and the resulting $G^{1/2}$ shows a nonlinear trend as expected: at high crack speed, the data collapses onto a master curve with that with $h_{\rm pen}/h_{\rm dc} \approx$ 0.2 (C = 0.024%), following $G_{\rm slip}^{1/2} \sim \ln V_{\rm crack}$ (Fig 2f). Note that in this regime, the slip linkage-mediated adhesion is higher than that mediated by stitch linkage for the same C between two regular gels (Fig 2f inset). Below $V_{\text{crack}}=0.5\text{mm/s}$, the data converges to a plateau corresponding to rate-independent adhesion energy of $\sim 50~\mathrm{Jm^{-2}}$. This baseline adhesion is also close to the value of G_{stitch} for the same C ($\sim 60 \text{ Jm}^{-2}$, Fig 2f inset), confirming the co-existence of stitch- and slip260

265

266

267

270

271

274

275

276

277

278

279

280

281

232

233

234

235

238

239

242

243

244

245

247

249

250

251

252

253

254

255

256

linkages on the interface. Fixing $G_{\rm stitch}=50~{\rm Jm}^{-2}$, our model captures the experimentally measured $G_{\rm hybrid}^{1/2}$ with fitting parameters $k_{\rm slip}=1\times 10^{-7}~{\rm N/m}$ and $E_{\rm slip}=71~{\rm kJ/mole}$ (Fig 2f, cyan dot line), closed to the values of the sample with $h_{\rm pen}/h_{\rm dc}\approx 0.2$ (C=0.024%). The ability to control the formation of linkage by tuning the entanglement length between TEA gel and bridging polymers offers a high level of adhesion programmability: not only can we predictably tune the adhesion energy by varying loading rates, but also program rate dependence in different ranges of loading rate. The finite adhesion energy at low loading rates provided by the hybrid linkage can effectively prevent the adhesive from failing at static load to ensure good durability.

286

288

289

290

291

292

293

294

295

296

297

298

301

302

303

304

305

306

307

309

310

311

312

313

315

316

317

318

319

320

321

322

323

324

325

326

327

331

332

333

334

335

336

337

338

339

340

341

342

343

Programming adhesion kinetics. In addition to the equilibrium state of adhesion, we next demonstrate that the association of the topological linkages regulates the transient adhesion, which can be exploited to encode adhesion kinetics (Fig 1d). When the bridging polymer solution is placed between the hydrogel and a permeable substrate, they diffuse into the two networks while simultaneously crosslinking into a bridging network in response to a trigger. The reaction-diffusion process comprises two concurrent sub-processes: the gelation and the diffusion of the bridging polymer with their kinetic time $t_{\rm gel}$ and $t_{\rm d}$, respectively. We assume that the overall adhesion kinetics is governed by the slower sub-kinetics: $t \equiv \max\{t_{\rm d}, t_{\rm gel}\}$.

When using chitosan as the bridging polymer, the gelation process is due to the decrease of pH, which is associated with the diffusion of gelling trigger (protons) away from the cast adhesive solution. The thickness of the solution $h_{\rm sol}$ sets the critical diffusion length, and thus its kinetics time follows $t_{\rm gel} \sim h_{\rm sol}^2/D_{\rm eff,gel}$ (32) where $D_{\rm eff,gel}$ is the effective diffusion coefficient of the gelling trigger. However, $h_{\rm sol}$ is sensitive to the applied compression or wettability of the interface, yielding the gelation kinetics uncertain in practice without carefully controlled $h_{\rm sol}$.

In contrast, the diffusion process of bridging polymers depends on the value of $h_{\rm dc}$, and hence the type of formed linkages. For a regular gel, $h_{\rm dc} \to 0$, the interface is dominated by stitch linkages which only require the bridging polymer to diffuse by one mesh size of the gel network, thus taking negligible kinetic time $t_d \approx 0$ s (32). As such, one can expect the adhesion kinetics of the regular hydrogel interface to be limited by $t_{\rm gel}$, which is difficult to control in practice due to the variable $h_{\rm sol}$. We hypothesize that incorporation of slip or hybrid linkages can resolve the issue. In this case, the formation of the linkages requires the bridging polymers to diffuse through the dangling chains layer (Fig 3a), and $h_{\rm dc}$ sets the characteristic diffusion length scale which yields $t_{\rm d} \sim$ $h_{\rm dc}^2/D_{\rm eff}$ where $D_{\rm eff}$ is the effective diffusion coefficient of the bridging polymers. The prolonged diffusion process can bypass the uncertain gelation process to govern the overall adhesion kinetics. Importantly, since h_{dc} is a material property, it can render the overall adhesion kinetics insensitive to processing or environmental conditions.

To test the hypothesis, we characterized the adhesion kinetics with different values of $h_{\rm sol}$ (50 and 120 μ m) controlled by nylon meshes of different thicknesses(32) (Methods and SI Appendix Fig. S6). We define the adhesion kinetics using the half time $t_{1/2}$ when G reaches half of the equilibrium state value $G_{\rm eq}$. For the regular gel interface, we observe a strong $h_{\rm sol}$ -dependent adhesion kinetics, and the associated kinetic

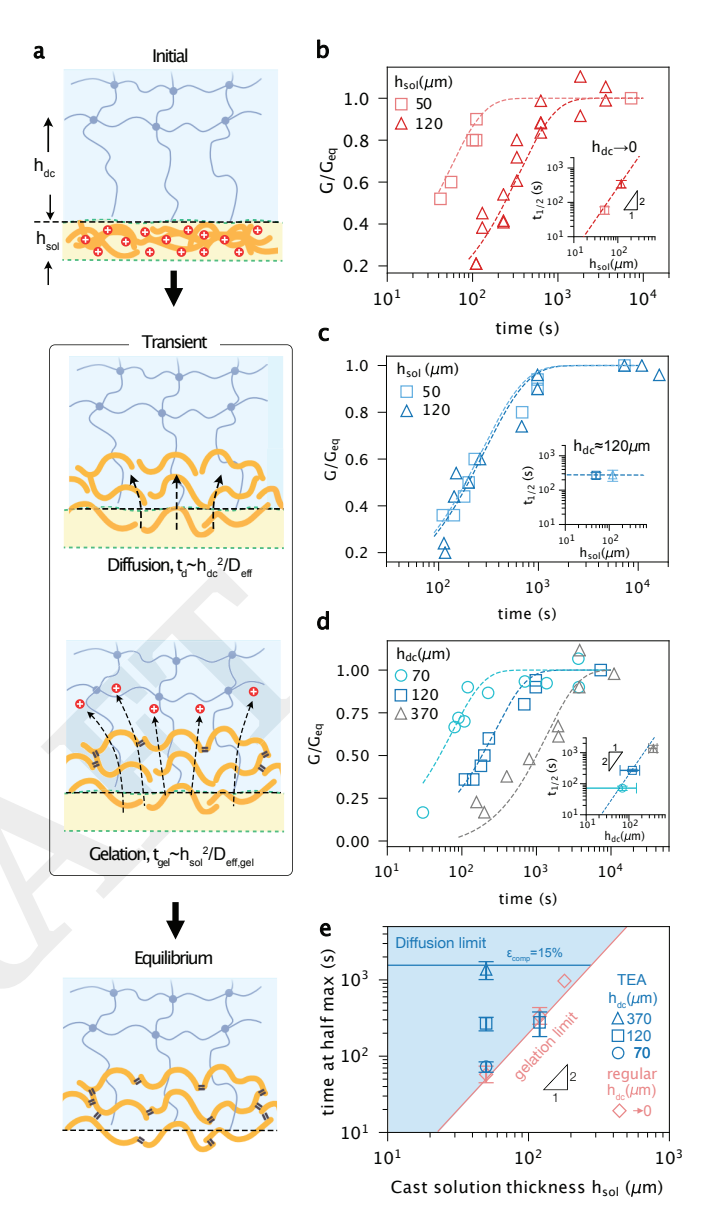


Fig. 3. Programmable adhesion kinetics of TEA.(a) Illustrations showing that the total adhesion kinetics comprises two sub-kinetic processes: diffusion and gelation. (b) Dimensionless adhesion between two regular hydrogels $G/G_{
m eq}$ with $G_{\rm eq}=49.98{\rm Jm}^{-2}$ and $47.42{\rm Jm}^{-2}$, as functions of waiting time for cast solution thicknesses $h_{\rm sol}=50\mu m$ and $120\mu m$, respectively. The inset shows $t_{1/2}$ as a function of $h_{
m sol}$. Error bars represent 95% confidence intervals from fitting the exponential function. (c) Similar curves as (b) measured at the interface between two TEA gels with $h_{\rm dc} \approx 120 \mu m.~G_{\rm eq} = 48.10 {\rm Jm}^{-2}$ and $47.4 {\rm Jm}^{-}$ $h_{\rm sol} = 50 \mu m$ and $120 \mu m$, respectively. (d) Adhesion kinetics of TEA interfaces with fixed $h_{\rm sol}$ $(50\mu m)$ and varying values of $h_{\rm dc}$ $(h_{\rm dc}\approx 370,120,70\mu m,$ achieved using $C=0.024\%,\,0.048\%,\,{\rm and}\,\,0.06\%,\,{\rm respectively}).$ $G_{\rm eq}=76.37{\rm Jm}^{-}$ $48.10 {
m Jm}^{-2}$ and $28.78 {
m Jm}^{-2}$, for $h_{
m dc} \approx 370, 120, 70 \mu m$, respectively. The inset shows $t_{1/2}$ as a function of $h_{
m dc}$. The y error bars represent a 95% confidence interval from fitting an exponential function while the x error bars represent the standard deviation from 3 measures. (e) $t_{1/2}$ for regular $(h_{
m dc} o 0)$ and TEA gels (varying $h_{\rm dc}$) plotted as functions of $h_{\rm sol}$. The blue horizontal line of corresponds to the TEA gel subject to an instantaneous compression of 15% strain without thickness-defining mesh (*SI Appendix* Fig S6c). The red diamond at $h_{\rm sol}=180\mu{\rm m}$ is adapted from reference (32).

time follows $t_{1/2} \sim h_{\rm sol}^2$ (Fig 3b and inset). On the contrary, we observe that the adhesion kinetics of the TEA gel interface with $h_{\rm dc} \approx 120 \mu m$ (C = 0.048%) is insensitive to the value of $h_{\rm sol}$ (Fig 3c and inset). Our point is further strengthened by applying an initial compression (15% strain) to the TEA gel interface ($h_{\rm dc} \approx 370 \mu m$) without controlling $h_{\rm sol}$, which yields the same adhesion kinetics as the TEA gel interface with controlled $h_{\rm sol}$ (SI Appendix Fig. S6c). Thus, incorporation of the engineered dangling chain layer leads to adhesion kinetics insensitive to processing conditions, validating our hypothesis.

347

348

349

350

353

354

355

356

357

358

359

360

361

362

363

366

367

368

369

370

371

372

373

374

375

376

379

380

381

382

383

387

388

389

390

391

392

394

395

396

397

400

401

402

403

404

405

Importantly, not only is the TEA kinetics insensitive to processing conditions, but also it is controllable through changing $h_{\rm dc}$. Fixing $h_{\rm sol}$, we observed strong $h_{\rm dc}$ -dependent adhesion kinetics of the TEA gel interface: the kinetics accelerates as $h_{\rm dc}$ decreases, suggesting shorter distance that the bridging polymers need to diffuse across to form hybrid or slip linkages (Fig 3d). The half time follows $t_{1/2} \sim h_{\rm dc}^2$ at $h_{\rm dc} \approx 70$ and 120 μ m. Fitting of the scaling relation to the data at these two $h_{\rm dc}$ values yields $D_{\rm eff} \approx 0.5 \times 10^{-12} {\rm m}^2 {\rm s}^{-1}$, agreeing reasonably well with the value predicted by Rouse model (Fig 3d inset, SI Appendix note 3). Our data, however, deviates from the scaling relation at $h_{\rm dc} \approx 370~\mu{\rm m}$ (Fig 3d inset). In the last case, the kinetics time is presumably bounded by the total diffusion-reaction time since $h_{\rm pen}/h_{\rm dc} \ll 1$, indicating that the underlying crosslinked network of the TEA gel is beyond the reach of bridging polymers.

Next, we discuss the role of each sub-kinetic process in determining the overall kinetics of TEA adhesion (Fig 3e). In principle, the overall adhesion kinetics is a function of two key parameters: $h_{\rm dc}$ and $h_{\rm sol}$, which govern the two sub-kinetics $t_{\rm d}$ and $t_{\rm gel}$, respectively, i.e., $t_{1/2} \equiv \max\{t_{\rm d}(h_{\rm dc}), t_{\rm gel}(h_{\rm sol})\}$ A simple scaling analysis allows determination of the critical condition at which the limiting kinetic mechanisms switch: $h_{\rm dc}^2 D_{\rm eff,gel}/h_{\rm sol}^2 D_{\rm eff} = 1$. Taking $D_{\rm eff,gel} \approx 10^{-11} \text{ m}^2 \text{ s}^{-1}$ (32) and using the estimated value of $D_{\rm eff} \approx 5 \cdot 10^{-12} \ {\rm m^2 \ s^{-1}}$ lead to $h_{\rm dc} \approx h_{\rm sol}$. When $h_{\rm dc} \gg h_{\rm sol}$ (the blue regime of Fig 3e), $t_{\rm d} \gg t_{\rm gel}$, so that the $t_{1/2}$ of TEA gel is solely dependent on $h_{\rm dc}$ through $t_{1/2} \equiv t_{\rm d} \sim h_{\rm dc}^2/D_{\rm eff}$. This allows us to tune the adhesion kinetics by varying $h_{\rm dc}$. On the other hand when $h_{\rm dc} < h_{\rm sol}$, the limiting kinetic mechanism switches due to $t_{\rm d} <$ $t_{\rm gel}$, so that the adhesion kinetics is tunable by varying $h_{\rm sol}$ through $t_{1/2} \equiv t_{\rm gel} \sim h_{\rm sol}^2/D_{\rm eff,gel}$. Therefore, the adhesion kinetics of the regular gels can be considered as a special case of TEA gels in the limit of $h_{\rm dc} \rightarrow 0$, where the dominating kinetic mechanism is the gelation of the bridging polymers (indicated by the red line in Fig 3e). The programmable TEA kinetics and can be tailored to suit different applications. For instance, a small $h_{\rm dc}$ can be used with compression to achieve fast kinetics for hemostatic applications (33), while a large $h_{\rm dc}$ provides a sufficient and adjustable time window for adhesive placement.

We further note that $h_{\rm dc}$ in this study is reduced by increasing C, which tends to embrittle the bulk and hence reducing the equilibrium adhesion energy $G_{\rm eq}$ of the TEA gel (Fig 3d). For certain applications that demand both fast and strong adhesion, one could vary $h_{\rm dc}$ independently of C by polymerizing gels on molds with different hydrophobicity. This approach could enable the tuning of adhesion kinetics without changing $G_{\rm eq}$. As a proof of concept, we demonstrate that a regular hydrogel, polymerized on a hydrophilic mold, contains negligible dangling chain layer $h_{\rm dc} \rightarrow 0$ regardless of the value of

C. Thus, a regular gel with relatively low crosslinking density C=0.024% shows both fast adhesion kinetics (\sim 70s with $h_{\rm sol}=50\mu{\rm m}$) and high $G_{\rm eq}$ (200 Jm⁻²) due to the combination of small h_{dc} and small C (SI Appendix Fig S6d). This strategy enables the formation of fast and strong adhesion simultaneously.

408

409

410

411

412

414

415

416

417

418

419

420

424

425

426

427

430

431

432

433

434

435

437

438

439

440

441

442

443

444

447

448

449

450

451

453

454

455

456

457

458

461

462

463

464

Universal applicability. The design and fabrication of TEA are universally applicable to a wide range of material systems, including various bridging polymers, targeted substrates, and TEA networks (Fig 4a). We first examine a different bridging polymer gelatin in addition to chitosan. Gelatin was prepared as polymer solution at $37^{\circ}C$ and then applied to the interface between two TEA gels for C=0.024% at room temperature. Similar to chitosan, gelatin diffused into the gel and was crosslinked into a bridging network in responding to a temperature drop to form slip linkages with the TEA dangling chains. Our data reveals an identical trend between the data obtained using gelatin and chitosan as bridging polymers (Fig 4b), highlighting the dominating role of polymer topology rather than material chemistry in the formation of slip linkages.

Second, slip linkages formed at the gel-bridging network interface can be coupled with other interactions that the bridging network can interact with the targeted substrates, such as slip, stitch linkages or covalent bonds (34). For instance, the triggered crosslinking and the abundant amino groups of chitosan chains provide numerous options to interact with diverse substrates through stitch linkage or covalent bonds (35). Based on the principle, slip-slip, slip-stitch, and slip-bond linkages were achieved between two TEA gels, between a TEA and a regular gel, and between a TEA gel and a VHB elastomer, respectively (SI Appendix Table S1). Our data reasonably collapse for the three linkage types to engage different targeted substrates (Fig 4c), suggesting that the overall adhesion behavior is dictated by the slip linkages while depending less on the types of interactions between the bridging network and targeted substrates. Without the slip linkage, the adhesion between two regular PAAm gels (stitch-stitch) and between a regular PAAm gel and a VHB elastomer (stitch-bond) show much less rate-dependence and higher magnitude (Fig 4C). These results validate the robustness of adhesion programming through the TEA strategy.

Lastly, we explore using double-network (DN) hydrogel as the TEA network, which exhibit much higher fracture toughness and adhesion (5, 21, 36, 37) due to background dissipation compared to single-network (SN) hydrogels. We tested alginate/PAAm and chitosan/PAAm hydrogels as representative materials. In both types of DN gels, alginate and chitosan are physically crosslinked macromolecules and do not covalently interfere with the PAAm network, we expect that the hydrophobic mold could produce surface dangling chains in the PAAm network within the DN gels. We confirmed the presence of the dangling chain layer in the surface of a alginate/PAAm hydrogel polymerized on hydrophobic substrate by EDTA treatment to remove calcium-alginate bonds followed by Atomic Force Microscopy (AFM) tests (SI Appendix Fig. S7a,b). We then examined the adhesion of TEA and regular DN gels that respectively polymerized on PMMA and glass molds on porcine skin (for a systematic study on different gelling molds, see SI Appendix Fig. S7c). We use chitosan as the bridging polymer and EDC/NHS reagent to form covalent bonds between chitosan and tissue surfaces (21). Our

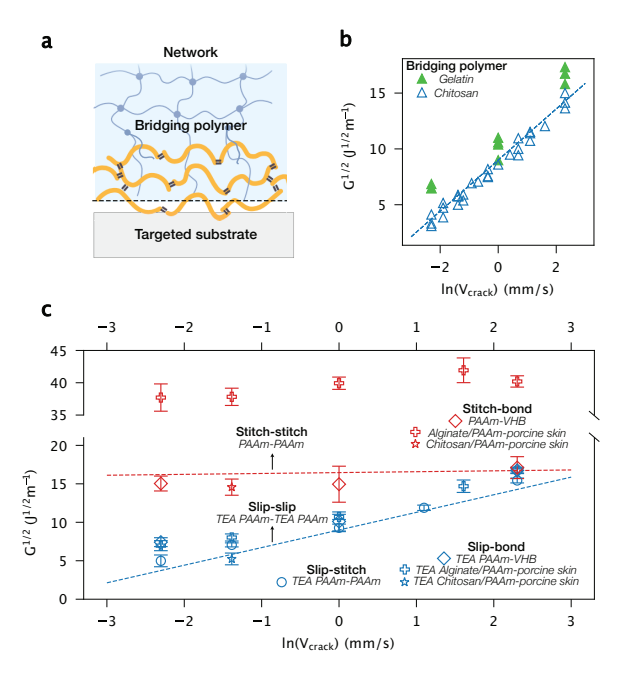


Fig. 4. Universal applicability of the TEA strategy. (a) Schematic showing that a TEA interface can be constituted by a variety of materials. (b) Slip-slip linage mediated adhesion between two TEA gels using gelatin and chitosan as bridging polymers. $c_{\rm chi} = c_{\rm gelatin} = 2\%$ g/ml (c) Topological linkages dictate hydrogel adhesion behaviors. The interfaces containing the slip linkage follow $G^{1/2} \sim \ln V_{\rm crack}$, and the adhesion shows stronger rate-dependence compared to those not containing the slip linkage. The red and blue dash lines correspond to the stitch-stitch and slip-slip-mediated adhesion in Fig 2d, respectively. The bridging polymer is chitosan with $c_{\rm chi} = 2\%$ g/ml. The TEA gels have crosslinker density C = 0.024%. The constituents of different topological linkages are listed in Table S1.

data shows that the adhesion of TEA alginate/PAAm gels on porcine skins (slip-bond) also follows $G^{1/2} \sim \ln V_{\rm crack}$, with similar slope to those of SN TEA gels (slip-slip, slip-stitch, and slip-bond) (Fig. 4c). In contrast, the adhesion between regular algiante/PAAm gels and porcine skins (stitch-bond) show much higher adhesion energy with less rate-dependence within the tested range of crack speed. Further investigations were conducted with TEA chitosan/PAAm gels on porcine skins (slip-bond) at $V_{\rm crack} = 0.25 \,\rm mm/s$, also agreeing with those of SN TEA gels. In comparison, the adhesion between regular chitosan/PAAm gels and porcine skins (stitch-bond) is almost 10-fold higher (37) than the TEA counterpart, consistent with the adhesion of SN regular gels (Fig. 4c). The results demonstrate that our methodology is not only applicable to SN hydrogels but also DN hydrogels as long as the topology of one of the networks can be engineered.

Programming spatial adhesion. The contrast between slip and stitch linkages allows us to program the adhesion spatially. To do so, we patterned a mold substrate with hydrophilic (Glass) and hydrophobic regions (PTFE films thickness \sim 0.1mm), followed by polymerizing a TEA gel on the patterned mold (SI Appendix Fig. S7d). While the unequal thicknesses of the hydrophilic and hydrophobic regions can influence the flatness of the resulting gel, we performed a separate experiment with varying thickness mismatch between the hydrophilic and hydrophobic regions (\pm 0.1mm) to confirm that the flatness does not affect the adhesion selectivity (SI Appendix Fig. S7e). Given the predefined geometries (circle, triangle) of the hy-

drophobic domains, we can design the dangling chain region where weak adhesion G_{slip} is formed at low loading rates; meanwhile, strong adhesion $G_{\rm stitch}$ is formed in other areas to sustain tension or twisting applied to the interface without interface debonding. Fig 5a and SI Appendix Fig. S7f show that by shaping the dangling chain region, we can achieve weak adhesion region of complex shapes between a TEA gel and a regular gel by slowly injecting liquid dye into the weak interface. To further characterize the resolution of the spatially programmable adhesion, we made a series of circular islands of nominal radii r_{nominal} in which slip linkages are formed. By slowly injecting the liquid dye, we visualized and measured their radii r_{measure} of the weak adhesion region using a digital camera (Fig. 5b). The excellent agreement between the nominal and measured radii suggests high spatial resolution ~ 0.1 mm achieved with a manual procedure. Moreover, the one-step fabrication allows spatially heterogeneous adhesion to be assembled within a piece of monolithic hydrogel, which otherwise requires assembling different materials at the interface. This could be conducted beforehand and using 3D-shaped substrates for curved adhesive surface. It is beneficial when soft, wet, and curved biological tissues are involved, as the hydrogel interface is inherently soft and mechanically compatible with such tissues. There exist other strategies such as selective masking for creating spatial heterogeneity in adhesion (13–15). Selective masking is a facile approach, but its implementation may involve the placement of masking materials, often made of rigid polymer films, which could be complicated by the mechanical mismatch and unwanted adhesion on soft, wet, rough and curved substrates such as biological tissues. Furthermore, substrate patterning procedures are time-consuming and may not suit time-sensitive scenarios such as surgical applications. In contrast, our method directly encodes the patterned adhesion into the soft and deformable hydrogel interface (38, 39), thereby alleviating the need for masking materials.

498

499

500

503

504

505

506

507

510

511

512

513

514

515

516

517

518

519

520

521

522

525

526

527

528

529

530

531

532

533

534

535

536

537

538

539

540

541

542

543

544

545

546

547

548

549

550

551

552

553

554

555

As the slip and stitch linkages show different sensitivities to loading rate, we expect the spatially selective adhesion, characterized by the adhesion energy contrast $G_{\rm slip}/G_{\rm stitch}$, to be also rate-dependent. Fig. 5c shows that $G_{\rm slip}/G_{\rm stitch}$ predicted by the parameterized model (SI Appendix note 2) approaches unity at high $V_{\rm crack}$ and decreases towards zero at low V_{crack} . The prediction is supported by our experimental observations: A TEA gel with the designed dangling chain region shows large adhesion contrast to a regular gel at low $V_{\rm crack}$, while the interface appears to be uniformly adhesive at relatively larger V_{crack} (Fig. 5d). The rate-dependent spatiallyprogrammable adhesion can potentially enable applications which desire tunable adhesion contrast in different regions under different loading rates. Additionally, not only we can achieve reduced adhesion $(G_{\text{slip}}/G_{\text{stitch}} < 1)$ but also enhanced adhesion $(G_{\text{hybrid}}/G_{\text{stitch}} > 1)$ in the engineered dangling chain region at large V_{crack} (SI Appendix Fig. S4b). In this case, the slip linkage acts as a toughener that synergistically contributes to the adhesion unit with the stitch linkage.

TEA-based devices. The programmable adhesion of TEA enables various applications such as wound patches, drug depots, fluidic channels, and soft actuators. For the application of wound patches, TEA allows for programming weak adhesion to wound beds while maintaining strong adhesion to the surrounding healthy tissue. As such, the patch could protect the wound without impairing tissue regeneration and wound

469

470

471

472

473

474

475

476

477

478

479

480

481

483

484

485

486

487

488

489

490

491

492

493

494

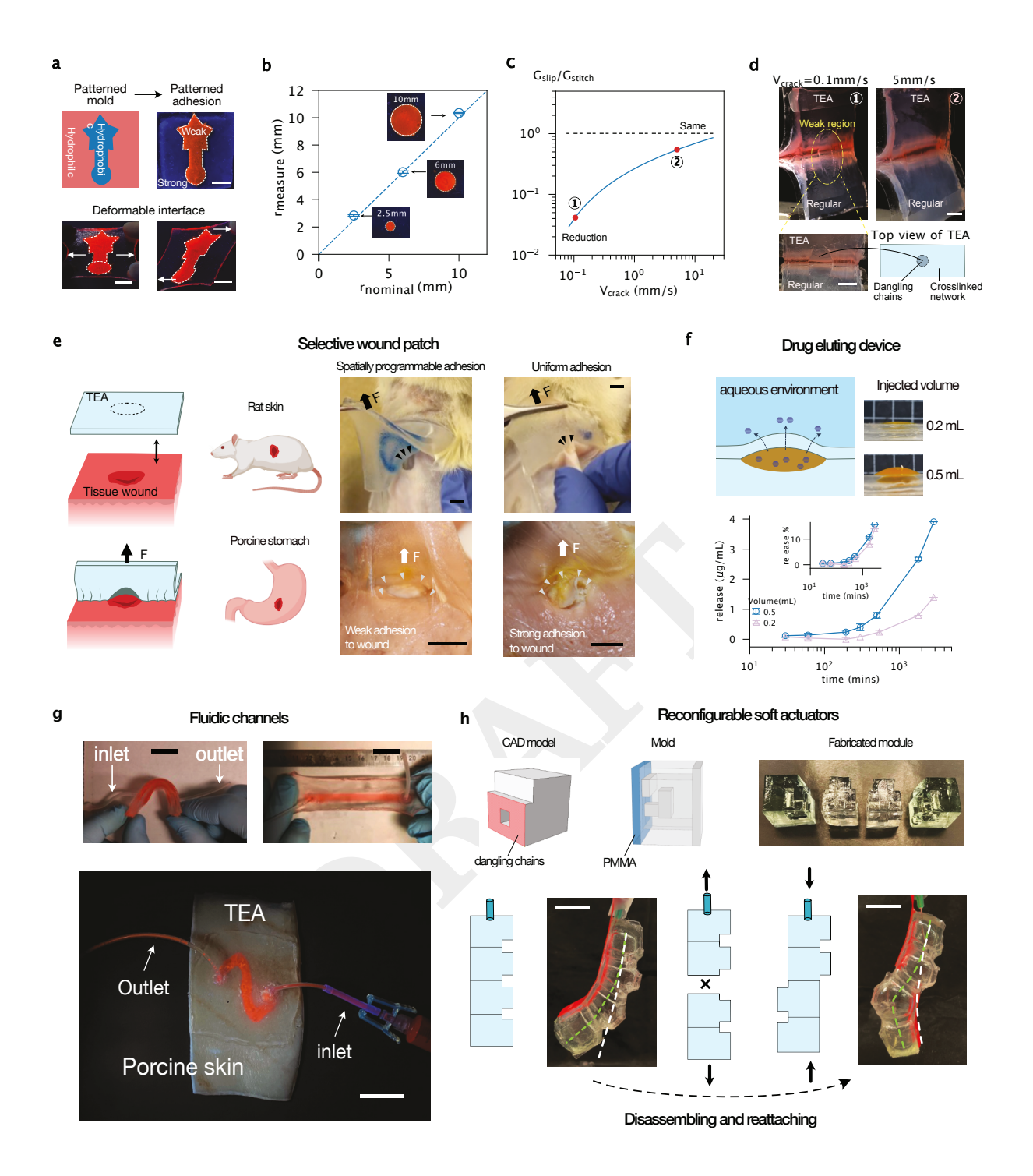


Fig. 5. Spatial programming and soft devices enabled with TEA (a) TEA strategy enables spatially programmable and deformable adhesion between a TEA alginate/PAAm gel and a regular alginate/PAAm gel. The patterned adhesion is visualized by slow injection of liquid dye into the weak interface. Scale bar: 1cm. (b) Spatial resolution of the spatially programmable adhesion. (c) Predicated adhesion energy contrast $G_{\mathrm{slip}}/G_{\mathrm{stitch}}$ achieved using the parameterized model (SI Appendix Eqn. S14) using the data of $G_{
m slip}$ and $G_{
m stitch}$ in Fig 2d. (d) Experimental demonstration of the rate-dependent $G_{
m slip}/G_{
m stitch}$ between a SN TEA gel with a circular-shaped dangling chain region and a SN regular gel. Scale bar: 1cm. (e) Wound patches made of TEA and regular alginate/PAAm gels adhered to wounds on rat skin (top, scale bar: 8mm) and porcine stomach (bot, scale bar: 12mm). (f) A drug-eluding device enabled by injecting drug into the weakly-adhered interface between a SN TEA gel and a SN regular gel. Grid size of the inset: 10mm. (g) Deformable hydrogel-based fluidic channels created by adhering a TEA alginate/PAAm gel to a regular alginate/PAAm gel. Scale bars: 2cm. (Bottom) A TEA alginate/PAAm gel with designed adhesion selectivity forms a fluid channel on the surface of a porcine skin. Scale bar: 2.5cm. (h) Reconfigurable soft actuators. (Top) the fabrication process of the actuator units with connection surfaces composed of dangling chains. (Bottom) two modes of actuation. The initial and the actuated stages are indicated by the white and green dash lines, respectively. Scale bars: 2cm.

closure. Using the one-step fabrication process (Fig 1e and SI Appendix Fig. S7d), we prepared such a TEA gel with its surface composed of a circular region of dangling chains and the surrounding region of crosslinked network. The dangling

558

chain region forms slip linkages which attach weakly to the wound site upon slow removal to minimize the damage to the wound. Meanwhile, the stitch linkages attach strongly to the surrounding healthy tissue to maintain the stickiness of the patch. In contrast, a regular hydrogel exerts strong and uniform adhesion to both wounded and healthy tissues, which ruptures the wound bed upon removal (Fig 5e).

562

563

564

565

568

569

570

571

572

576

577

578

579

582

583

584

585

587

590

591

592

593

594

595

596

597

598

599

600

601

602

603

605

607

608

609

610

611

613

614

615

616

618

Besides, the creation of a weak adhesion region between two hydrogels could serve as a drug depot. Upon slow injection, mock drug solution filled up the weak interface. Further injection created a bulge of hydrogel to accommodate a high amount of drug, which can be continuously released through the hydrogel network when the whole device is immersed in an aqueous environment (Fig. 5f Top). Our data show that the initial amount of drug injected into the depot affects the amount of release over time but the relative kinetics of release remains similar (Fig. 5f Bottom). As well, we can create a drug depot above a wound site, where drugs can be directly released into wounded tissue. In contrast, the strong adhesion of a regular hydrogel prevents the injection of drug solution to interface (SI Appendix Fig. S7g).

We then demonstrate hydrogel-based fluidic devices assembled with TEA. A PAAm-alginate TEA DN gel with a rectangular-shaped dangling chain region forms a partially weak interface with a regular DN gel, which subsequently becomes a fluidic channel upon slow injection of liquids. The resulting device is highly deformable while no liquid leakage is observed (Fig 5g Top). The one-step fabrication technique provides a simple approach to fabricate hydrogel fluidic channels compared with conventional methods that typically involve multiple molding steps (40, 41). In addition, the spatially programmable adhesion is applicable to varying surfaces as it requires no patterning of the targeted substrate. As such, we can form such a fluid channel directly on tissue surfaces such as porcine skin (Fig 5g Bottom). This feature could benefit medical devices that contact with tissue surfaces for sustained drug release (42), or in-vitro organ-on-chip models to study cellular behaviors (43).

Lastly, we show that the TEA made of SN PAAm hydrogels can be used to construct reconfigurable soft actuators, featuring minimal bulk dissipation for efficient actuation and dynamic adhesion for reversible attachment (Fig 5h). Such actuators are formed with hydrogel units that contain surface dangling chains on each face and are connected to each other with the aid of bridging polymer (Methods). The slip linkage-mediated adhesion between the units is strong enough to sustain actuation, and yet can be separated easily and slowly with a small force. The separated units can then be reconnected upon reapplying the bridging polymer solution to the interface so that one can modify configurations of assembly for different actuation. Our data shows that the slip linkage-mediated adhesion increases and reaches a plateau after cycles of detachment and reattachment (SI Appendix Fig. S5d). This property can be partially attributed to the fact that the dissociation of the slip linkage only involves chain slippage, hence not rupturing the adherend networks (SI Appendix Fig. S5e). Thus, the slip-mediated TEA interface is inherently subjected to minimal damage compared with those bonded by stitch linkages or covalent bonds.

Conclusion

In summary, we have demonstrated that designing the interfacial network topologies of hydrogels provides a facile and robust approach to program adhesion in multiple aspects including magnitude, space, and kinetics. Our approach can be potentially extended to different length scales using proper manufacturing processes. For instance, spatially programmable adhesion with a spatial resolution on the micro-scale can be achieved with microfabrication of the hydrogel network topology (44, 45), while that on the metre scale is expected to be achieved using gelling molds of the same size for applications such as camouflaging skin (46). Broadly, our methodology falls into the emerging paradigm of material intelligence, as the adhesion programming is directly encoded in the hydrogel network as material properties, similar to other properties such as elastic modulus. The implementation of adhesion control requires no external apparatus, making the methodology extremely facile, robust, and scalable. We hope that the design of TEA can spark interest in controlling hydrogel adhesion by designing their network topologies, opening the door to a new design space for intelligent materials/structures through programmable adhesion.

622

623

624

626

627

628

629

630

631

634

635

636

637

638

639

640

641

642

643

644

645

646

648

649

650

651

652

653

654

655

656

657

658

659

660

661

662

663

664

665

666

667

668

669

670

671

672

673

674

675

676

678

679

680

681

682

683

684

685

Materials and Methods

Materials. All chemicals were purchased and used without further purification. Materials for the hydrogel synthesis and the bridging polymer include acrylamide (AAm, Sigma-Aldrich, A9099), N,N'-methylenebisacrylamide (MBAA; Sigma-Aldrich, M7279), ammonium persulphate (APS, Sigma-Aldrich, A3678), N,N,N',N'tetramethylethylenediamine (TEMED, Sigma-Aldrich, T7024), Alginate (I-1G) was purchased from KIMICA Corporation, chitosan (degree of deacetylation, DDA: 95%, medium and high molecular weight, Lyphar Biotech), sodium bicarbonate (Fisher Scientific, S233), sodium phosphate monobasic (NaH2PO4, Sigma, S8282), sodium phosphate dibasic (Na2HPO4, Sigma-Aldrich, S7907), acetic acid (Sigma-Aldrich, A6283), calcium sulfate (Sigma-Aldrich), N-hydroxysulfosuccinimide (NHS, Sigma-Aldrich, 130672), and 1-ethyl-3-(3-dimethylaminopropyl) carbodiimide (EDC, Sigma-Aldrich, 03450), Gelatin (Sigma-Aldrich, G2500). Glass, acrylic sheets (PMMA), PS, silicon, and PTFE were purchased from McMaster-Carr to make mold substrates for polymerization. VHB elastomer was purchased from 3M. Porcine skin was purchased from a local grocery store, then stored in a fridge at -20 $^{\circ}$ C, and thawed at 4°C before use. Nylon mesh were purchased from McMaster Carr without further modification (9318T25, 9318T23 for thicknesses of $50 \ \mu m$ and $120 \ \mu m$, respectively.)

Synthesis of TEA. The single network PAAm TEA gels were prepared as follows. AAm monomers of 6.76 g was first dissolved in 50 mL of deionized water. After degassing, the AAm solution of 25 ml was mixed with varying amounts of MBAA aqueous solution (0.02 g mL⁻¹) and 20 μ L of TEMED in a syringe. The volumes of MBAA solution added were 90, 120, 150, 180, and 240 μL for the crosslinker-to-monomer molar ratios C at 0.024%, 0.032%, 0.04%, 0.048%, 0.06%, respectively. Meanwhile, another syringe was added with 565 μL of APS solution (0.066 g mL⁻¹) and 478 μL deionized water. The two syringes were connected with a Luer-Lock connector, so the two solutions were syringe-mixed to form a homogeneous solution. The mixture was immediately injected into rectangular acrylic molds of $80 \times 20 \times 3 \text{ mm}^3$ or $80 \times 15 \times 1.5$ mm³, covered with PMMA on both sides, and then kept at room temperature for 24 hours to complete the reaction. To prepare the regular PAAm gels, we follow the same procedure except for injecting the mixed solution into the acrylic molds covered by glass sheets on the two sides. The synthesis of double network TEA gels is similar to that for the single network TEA gels, and is detailed in SI Appendix.

Preparation of the bridging polymer solutions. This study tested two types bridging polymers: chitosan and gelatin. To prepare the chitosan solutions of 2%, 1%, and 0.5% w/v, 50 mL of deionized water was added with chitosan powders of 1, 0.5, 0.25 g, respectively. $400~\mu L$ of acetic acid was also added for a final pH of 4.5. The mixture was stirred overnight to form a homogeneous solution and then kept at 4°C before use. To prepare the gelatin solution of 2% w/v, 1g of gelatin powder was dissolved in 50 mL of deionized water. The solution was stirred in a water bath at $37^{\circ}C$ for 30 mins before

686

687

688

689

690

691

692

693

694

696

697

700

701

702

703

704

705

706

707

708

709

710

711

712

713

714

715

716

717

718

719

720

721 722

723 724

725

726

727 728

729

730 731

732

733

734 735

736

737

738

739

740

741 742

743 744

745 746

747

748

749

750 751

752

753 754

755

756

757

758

760

761 762

All details associated with sample preparations, mechanical tests, derivation and calibration of the thermally activated chain slippage model, estimation of the diffusion coefficients of bridging polymers can be found in SI Appendix

ACKNOWLEDGMENTS. This work is supported by the Natural Sciences and Engineering Research Council of Canada (grant RGPIN-2018-04146), Fonds de Recherche du Quebec-Nature et technologies (grants FRQNT PR-281851), and the National Institute on Deafness and Other Communication Disorders (grant R01-DC018577). Z.Y. and R.H. acknowledge support from FRQNT and McGill Engineering Doctoral Award. S.J. acknowledges support from FRQNT Doctoral Award. X.Y. and R.L. acknowledge support from the National Science Foundation of the United States (NSF CMMI-1752449). J.L. acknowledges the support from the Canada Research Chair Program. The authors acknowledge Mr. Tianqin Ning and Mr. Yixun Chen for taking pictures, Mr. Omar Peza-Chavez for helping with cryosectioning.

- Z Yang, X Yang, R Long, J Li, Stimulation modulates adhesion and mechanics of hydrogel adhesives. Langmuir 37, 7097-7106 (2021).
- H Cho, et al., Intrinsically reversible superglues via shape adaptation inspired by snail epiphragm. Proc. Natl. Acad. Sci. 116, 13774-13779 (2019).
- AB Croll, N Hosseini, MD Bartlett, Switchable adhesives for multifunctional interfaces. Adv. Mater. Technol. 4, 1900193 (2019).
- S Blacklow, et al., Bioinspired mechanically active adhesive dressings to accelerate wound closure. Sci. advances 5, eaaw3963 (2019).
- H Yuk, T Zhang, S Lin, GA Parada, X Zhao, Tough bonding of hydrogels to diverse non-porous surfaces. Nat. Mater. 15, 190-196 (2016).
- X Chen, H Yuk, J Wu, CS Nabzdyk, X Zhao, Instant tough bioadhesive with triggerable benign detachment. Proc. Natl. Acad. Sci. 117, 15497-15503 (2020).
- J Yang, R Bai, Z Suo, Topological adhesion of wet materials, Adv. Mater. 30, 1800671 (2018).
- Y Gao, K Wu, Z Suo, Photodetachable adhesion. Adv. Mater. 31, 1806948 (2019)
- Z Ma, et al., Controlled tough bioadhesion mediated by ultrasound. Science 377, 751-755
- 10. Y Wang, et al., Instant, tough, noncovalent adhesion. ACS Appl. Mater. & Interfaces 11, 40749-40757 (2019)
- EP Chan, D Ahn, AJ Crosby, Adhesion of patterned reactive interfaces, The J. Adhesion 83. 473-489 (2007). JM Dugan, C Colominas, AA Garcia-Granada, F Claeyssens, Spatial control of neuronal
- adhesion on diamond-like carbon. Front. Mater. 8, 756055 (2021).
- H Yuk, T Zhang, GA Parada, X Liu, X Zhao, Skin-inspired hydrogel-elastomer hybrids with robust interfaces and functional microstructures, Nat. communications 7, 12028 (2016).
- W Lee, J Lim, J Kim, Conformal hydrogel-skin coating on a microfluidic channel through microstamping transfer of the masking layer. Anal. Chem. 95, 8332-8339 (2023).
- 15. DC Young, IG Newsome, J Scrimgeour, Incorporation of soft shaped hydrogel sheets into microfluidic systems using a simple adhesion masking process. Appl. Phys. Lett. 111, 263705
- S Rakshit, Y Zhang, K Manibog, O Shafraz, S Sivasankar, Ideal, catch, and slip bonds in cadherin adhesion. Proc. Natl. Acad. Sci. 109, 18815-18820 (2012).
- V Barsegov, D Thirumalai, Dynamics of unbinding of cell adhesion molecules: transition from catch to slip bonds. Proc. Natl. Acad. Sci. 102, 1835-1839 (2005).
- RP McEver, C Zhu, Rolling cell adhesion. Annu. review cell developmental biology 26, 363-396 (2010)
- PW Oakes, S Banerjee, MC Marchetti, ML Gardel, Geometry regulates traction stresses in adherent cells. Biophys. journal 107, 825-833 (2014).
- ME Berginski, EA Vitriol, KM Hahn, SM Gomez, High-resolution quantification of focal adhesion spatiotemporal dynamics in living cells. PloS one 6, e22025 (2011)
- J Li, et al., Tough adhesives for diverse wet surfaces. Science 357, 378-381 (2017).
 - JP Gong, A Kii, J Xu, Y Hattori, Y Osada, A possible mechanism for the substrate effect on hydrogel formation. The J. Phys. Chem. B 105, 4572-4576 (2001).
- A Kii, J Xu, JP Gong, Y Osada, X Zhang, Heterogeneous polymerization of hydrogels on hydrophobic substrate. The J. Phys. Chem. B 105, 4565-4571 (2001).
- J Mandal, K Zhang, ND Spencer, , et al., Oxygen inhibition of free-radical polymerization is the dominant mechanism behind the "mold effect" on hydrogels. Soft Matter 17, 6394-6403 759
 - K Zhang, R Simic, W Yan, ND Spencer, Creating an interface: rendering a double-network hydrogel lubricious via spontaneous delamination. ACS Appl. Mater. & Interfaces 11, 25427-

MK Chaudhury, Bate-dependent fracture at adhesive interface. The J. Phys. Chem. B 103. 6562-6566 (1999)

763

764

765

766

767

768

769

770

771

772

773

774

775

776

777

778

779

780

781

782

783

784

785

786

787

788

789

790

791

792

793

794

795

796

797

798

799

800

801

- E Evans, K Ritchie, Dynamic strength of molecular adhesion bonds. Biophys. J. 72, 1541-1555 (1997)
- 28. GI Bell, Models for the specific adhesion of cells to cells; a theoretical framework for adhesion mediated by reversible bonds between cell surface molecules. Science 200, 618-627 (1978).
- 29. IV Pobelov, et al., Dynamic breaking of a single gold bond. Nat. communications 8, 15931 (2017).
- C Creton. M Ciccotti, Fracture and adhesion of soft materials: a review. Reports on Prog. 30. Phys 79 046601 (2016)
- 31. S Wang, S Panyukov, M Rubinstein, SL Craig, Quantitative adjustment to the molecular energy parameter in the lake-thomas theory of polymer fracture energy. Macromolecules 52, 2772-2777 (2019).
- J Steck, J Kim, J Yang, S Hassan, Z Suo, Topological adhesion. i. rapid and strong topohesives. Extrem. Mech. Lett. 39, 100803 (2020)
- G Bao, et al., Liquid-infused microstructured bioadhesives halt non-compressible hemorrhage. Nat. Commun. 13, 5035 (2022)
- J Yang, R Bai, B Chen, Z Suo, Hydrogel adhesion: a supramolecular synergy of chemistry, topology, and mechanics. Adv. Funct. Mater. 30 (2019).
- J Yang, et al., Design molecular topology for wet-dry adhesion. ACS Appl. Mater. & Interfaces 11, 24802-24811 (2019).
- JY Sun, et al., Highly stretchable and tough hydrogels. Nature 489, 133-136 (2012).
- G Bao, et al., lonotronic tough adhesives with intrinsic multifunctionality. ACS Appl. Mater. & Interfaces 13, 37849-37861 (2021)
- X Liu, J Liu, S Lin, X Zhao, Hydrogel machines. Mater. Today 36, 102-124 (2020).
- J Yang, J Steck, R Bai, Z Suo, Topological adhesion ii. stretchable adhesion. Extrem. Mech. Lett. 40, 100891 (2020)
- 40. N Gjorevski, et al., Tissue geometry drives deterministic organoid patterning. Science 375. eaaw9021 (2022).
- S Lin, et al., Stretchable hydrogel electronics and devices. Adv. Mater. 28, 4497-4505 (2016).
- W Whyte, et al., Sustained release of targeted cardiac therapy with a replenishable implanted epicardial reservoir. Nat. Biomed. Eng. 2, 416-428 (2018)
- 43. D Vera, et al., Engineering tissue barrier models on hydrogel microfluidic platforms. ACS Appl. Mater. & Interfaces 13, 13920-13933 (2021).
- 44. A Tudor, et al., Fabrication of soft, stimulus-responsive structures with sub-micron resolution via two-photon polymerization of poly (ionic liquid)s. Mater. Today 21, 807-816 (2018).
- M Carlotti, V Mattoli, Functional materials for two-photon polymerization in microfabrication. Small 15, 1902687 (2019).
- 46. J Pikul, et al., Stretchable surfaces with programmable 3d texture morphing for synthetic camouflaging skins. Science 358, 210-214 (2017).

PNAS

Supporting Information for

- Programming hydrogel adhesion with engineered polymer network topology
- ⁴ Z Yang, G Bao, R Huo, S Jiang, X Yang, X Ni, L Mongeau, R Long, and J Li
- 5 Jianyu Li.
- 6 E-mail: jianyu.li@mcgill.ca

7 This PDF file includes:

- Supporting text
- 9 Figs. S1 to S9
- Table S1
- SI References

Supporting Information Text

Note 1: TEA gel prepared by heterogeneous polymerization

We consider here the heterogeneous structure of the TEA gel imparted by the hydrophobic mold substrate. The phenomenon was first discovered by Gong et al.(1–3), who proposed that the hydrophobic mold substrate suppresses the polymerization of the precursor solution near the substrate-solution interface due to the increased interfacial tension. When the pre-gel solution starts polymerizing on the low-surface-tension mold such as PMMA, the interfacial tension between the hydrophobic mold surface and the liquid solution γ_{sl} increases with the increased polymer fraction. To minimize the free energy of the whole system, the mold surface repulses the polymers to create a depletion layer of thickness ξ_{dp} , where the polymer fraction is significantly reduced compared to that in the bulk. As the polymerization continues, the polymer chains in the bulk start to entangle and from a crosslinked network with the bulk network elasticity E_{bulk} . Within the depletion layer, however, the crosslinking process is influenced due to the extremely low polymer fraction, resulting in a layer of dangling chains of thickness h_{dc} . We shall consider ξ_{dp} and h_{dc} to be equivalent. In equilibrium, the increased interfacial energy $\Delta \gamma_{sl}$ equals the work done against E_{bulk} over the distance ξ_{dp} , leading to the relation $\Delta \gamma_{sl} \sim E_{bulk} \xi_{dp}$ or $\Delta \gamma_{sl} \sim E_{bulk} h_{dc}$. By assuming γ_{sl} changes negligibly with E_{bulk} when C is varied, and all the crosslinkers effectively contribute to load-bearing chains, it leads to the scaling relation: $h_{dc} \sim 1/E_{bulk} \sim 1/C$, which is plotted in Fig. 2c with the estimated h_{dc} values.

Recently, several results suggested that the inhibition of free-radical polymerization by trapped oxygen on hydrophobic substrates may play significant roles in the heterogeneous polymerization (4, 5). Despite the debates on the underlying mechanisms, the substrate effect effectively produces heterogeneous structure of a TEA gel that comprises a layer of branched dangling chains spanning a thickness of h_{dc} near the surface, and a homogeneously crosslinked bulk network that is affected minimally by the substrate effect of thickness $h - 2h_{dc}$ (considering the gel is polymerized between two hydrophobic molds).

Indication of dangling chain layer in TEA gels using cryosectioning and SEM imaging. We performed cryosectioning of TEA and regular SN PAAm gels with C=0.024% into sheets of 100 μ m thickness, and dehydrated the sheets in the open air (Fig S3). The top and bottom edges of the TEA gel sheet are composed of branched dangling chains. Using SEM imaging, we observed that the two edges of the section shrink more than the center, forming a "ridge" with the downhill portion spanning over $\sim 400\mu$ m to $\sim 600\mu$ m(Fig S3 b, d). We attribute the significant shrinkage near the edge to the low polymer content and crosslinking density in the dangling chain layer compared to the bulk, causing more volume change during the process of dehydration. In contrast, a cryosectioned regular gel sheet shows a smaller edge shrinkage with size $< 200\mu$ m (Fig S3 c, e), which is presumably due to the inhomogeneous de-swelling resulted from the bottom confinement by the glass slide (6). The different amounts of edge shrinkage in TEA and regular gel sheets indicate that the edges of the TEA gel is composed of dangling chains. The dangling chain layer thickness $h_{\rm dc}$ is characterized using uniaxial tensile and micro-indentation tests, detailed below

Estimation of h_{dc} using uniaxial tensile test. We propose a simple model to characterize the value of h_{dc} of TEA gels. The model considers the TEA gel has an effective modulus of E_{tea} , composed of the bulk elastic modulus E_{bulk} and the dangling chain elastic modulus E_{dc} . It assumes that the bulk of the TEA gel the same elasticity E_{bulk} as that of a regular gel polymerized on glass E_{reg} , while the dangling chains has a modulus $E_{dc} \approx 0$, yielding:

$$\frac{2h_{\rm dc}}{h} = 1 - \frac{E_{\rm tea}}{E_{\rm reg}} \tag{1}$$

where E_{tea} and E_{reg} can be measured from uniaxial tensile tests. We fit the data with 5% of strain to the linear-elastic model, which is degenerated to from the neo-Hookean model at the small strain limit:

$$\sigma_{\text{linear}} = E(\lambda - 1)$$
 [2]

where σ is the nominal stress and λ is the stretch. We also fit the data to another hyperelastic material model, the incompressible neo-Hookean model:

$$W_{\text{neo-Hookean}} = \frac{E}{6}(I_1 - 3) \tag{3}$$

where $I_1 = \lambda_1^2 + \lambda_2^2 + \lambda_3^2$. The Neo-Hookean model assumes that the polymer chains follow Gaussian distribution and are free of entanglements. Under uniaxial tensile test, the principle stretches: $\lambda_1 = \lambda$, $\lambda_2 = \lambda_3 = 1/\sqrt{\lambda}$. The nominal stress-stretch curves derived from the models are:

$$\sigma_{\text{neo-Hookean}} = \frac{E}{3}(\lambda - \lambda^{-2})$$
 [4]

We plot representative stress-stretch curves from uniaxial tensile tests in Fig. S1 e and along with the fitted models. The Neo-Hookean model underestimates the slopes of the curves at $\lambda \to 1^+$ for all samples. The linear model that fit the data within λ from 1 to 1.05 is used to estimate the moduli of TEA and regular gels with varying values of C, plotted in Fig. S1 e. With the values of E_{tea} and E_{reg} , we estimated the value of h_{dc} using the Eqn. 1. Note that our estimation of h_{dc} is much larger than those estimated by observing force-displacement curves from nano-indentation tests(4)(7), which may attribute to the different values of C used in the studies. The projection of our data yields a similar estimation of h_{dc} at the same level of C as in Simic et al(4) ($C \approx 1\%$).

Estimation of h_{dc} using micro-indentation test. We further performed micro-indentation test to ascertain the value of h_{dc} using a custom built microindenter (Fig S2a and Methods). Fig S2 b and c illustrate the indentation test on the regular and TEA gels.

It has been shown that the bulk network of TEA gels has similar moduli E_{bulk} as those of regular gels, but the modulus of the dangling chain layer E_{dc} is much smaller: $E_{\text{dc}} \ll E_{\text{bulk}}$ (8). Thus the force-displacement curve of the TEA gel under indentation is expected to show a displacement delay δ_{delay} compared to that of the regular gel due to the soft dangling chain layer. Such displacement delay can be used as an indicator of the dangling chain thickness h_{dc} . For example, if $E_{\text{dc}}/E_{\text{bulk}} \to 0$, we expect $\delta_{\text{delay}} \approx h_{\text{dc}}$ (Fig S2 c). Fig S2 d shows that at large indentation depth, the force-displacement curves of all samples follow the scaling of $f \sim \delta^{3/2}$, indicating that the contacting behavior is Hertzian. At smaller indentation depths, the curves deviate from Hertzian contact presumably due to the adhesion between the gel surface and the indenter, resulting in JKR type of contact. Adhesion is also evidenced by our observation of a slight negative indentation force (i.e., tensile force) on the order of -200 μ N as the indenter was approaching the substrate surface. This is the pull-in behavior where adhesion deforms the substrate to establish contact with the indenter. Given that the distance range of adhesive interaction (e.g., van der Waals forces) causing the pull-in event is much smaller than the range of indentation displacement ($\delta > 100\mu$ m), we identify the pull-in event as the zero point for the indentation displacement. This condition is also adopted in other soft contact experiments (9). The curve of the regular gel with C = 0.048% follows Hertzian contact even at small indentation depths, likely due to its higher modulus reducing the relative effect of adhesion (10).

Fig S2 d also shows a displacement delay between TEA and regular gels as expected, with $\delta_{\rm delay}\approx 130\mu{\rm m}$ and $50\mu{\rm m}$ for C=0.024% and 0.048%, respectively. By shifting the indentation displacement δ of the TEA gels using their respective $\delta_{\rm delay}$ values, the force-displacement curves of TEA and regular gels collapse onto each other, indicating that the bulk networks in TEA and regular gels have similar moduli $E_{\rm bulk}$ (Fig S2 e). The ratio of $\delta_{\rm delay}/h_{\rm dc}\approx 0.4$ is consistent for both C values (Fig S2 f) but is less than 1, suggesting that the dangling chain layer has a non-zero modulus when it is under compression. It has been shown that a layer of polymer brush can exhibit strong lateral compression stress due to the excluded volume effect (11), and behaves as nonlinear springs in compression (12) with a reported compressive modulus of 0.3kPa for varying grafting densities (13). As such, we expect that $E_{\rm dc}$ of the dangling chain layer to be non-zero when being compressed perpendicular to the dangling chain layer, but negligible when loaded in tension parallel to the dangling chain layer, as assumed in our uniaxial tensile test.

To provide an estimation of $E_{\rm dc}$, we performed finite element (FE) modeling (Methods) to simulate the indentation of a layered material with the "bulk" and "dangling chain" regions of 2.63 mm and 0.37 mm, respectively, mimicking the structure of TEA gel at C = 0.024% (Fig S2 g). We vary $E_{\rm dc}/E_{\rm bulk}$ from 0 to 1 and extract $\delta_{\rm delay}$ by comparing the force-displacement curves (Fig S2h). The ratio $\delta_{\rm delay}/h_{\rm dc} = 1$ when $E_{\rm dc}/E_{\rm bulk} = 0$, and decreases rapidly as $E_{\rm dc}/E_{\rm bulk}$ increases, finally reaching 0 when $E_{\rm dc}/E_{\rm bulk} = 1$ (Fig S2i). Using an exponential fitting function $\delta_{\rm delay}/h_{\rm dc} = A \cdot \exp{(-E_{\rm dc}/E_{\rm bulk})/B}$ with A and B being fitting parameters, we find that $E_{\rm dc}/E_{\rm bulk} \approx 0.14$ when $\delta_{\rm delay}/h_{\rm dc} \approx 0.4$. Consequently, this suggests that $E_{\rm dc} = 0.58$ kPa and 1.05 kPa for C = 0.024% and 0.048%, consistent with the compressive modulus of polymer brush swollen in viscous solvent tested in a quasi-static condition (0.3 kPa (13)).

Estimation of bulk mesh size. Assuming the bulk network of the TEA gel and that of a regular gel have affine structures, so their shear modulus can be expressed as

$$\mu = \frac{E}{3} = \nu k_B T \tag{5}$$

where the density of the network strands $\nu = \frac{c_{\text{aam}}}{m_{\text{mono}}N_c}N_A$. The concentration of the aam solution is $c_{\text{aam}} = 6.76\text{g}/50 \times 10^{-6}\text{m}^3 = 1.352 \times 10^5 \text{ g/m}^3$. The molar mass of aam is $m_{\text{mono}} \approx 71 \text{ g/mole}$. Using the shear modulus of the regular PAAm gels for C = 0.024%, the number of monomers between two crosslinkers are approximated as:

$$N_c = \frac{c_{\text{aam}}}{m_{\text{mono}}\mu} N_A = \frac{c_{\text{aam}}}{m_{\text{mono}}\mu/k_B T} N_A \approx 2348$$
 [6]

The mesh size is thus estimated as:

$$\xi = aN_c^{1/2} = 0.1 \times N_c^{1/2} \approx 5$$
nm [7]

where $a \approx 0.1$ nm is the length of a single bond.

Alternative approaches to create slip-linkage topology. Other approaches exist to create the similar chain-network topology of the slip linkage, such as by placing uncrosslinked polymer chains between hydrogel networks(14, 15). The polymer chains can diffuse into the pre-formed gel networks to form slip entanglement. However, the highly permeable hydrogel would promote the diffusion of polymer chains into the gel matrix, greatly reducing the number of polymer entanglements on the interface.

Note 2: Thermally activated processes of chain slippage and ruptures

In experiments, we observed that $G^{1/2}$ for TEAs varies logarithmically with V_{crack} (Fig 2d and f) if $h_{pen}/h_{dc} \ll 1$, reminiscent of the dynamic adhesion of cell-cell interface(16), elastomer(17), and other bonds(18) due to thermally activated bond breaking. To rationalize the results, we adopt a kinetic theory which considers the linkage dissociation as thermally-activated processes(17, 19).

The activation for the dangling chain to slip from the bridging network is assumed to decrease by the applied force (Fig 2e).

Using the concept of mechanochemistry, the rate of dissociation of linkage *i* can be expressed as:

$$r_i(t) = -\frac{dN_i}{dt} = r_i N_i \tag{8}$$

where i can be stitch or slip. N_i is the areal density of linkage i, and r_i is the rate constant for linkage dissociation, and is assumed to be dependent on the force applied to the chains F via the Arrhenius law:

$$r_i = r_0 \exp\left(\frac{l_a F}{k_B T}\right) \tag{9}$$

where $r_0 = 1/\tau_-$ is the rate constant of the linkage dissociation without adding any force, τ_- is the intrinsic relaxation time of the slip linkage, k_BT is the temperature in the unit of energy, F is the applied force to break a linkage. Note that we have assumed the linkage dissociation process is irreversible, thus the re-association of the linkage is not accounted for. We further consider an individual linkage has a spring constant k_i and is stretched at a fixed velocity V over an averaged bond survival time $\bar{t_i}$. Thus, the averaged force that an individual linkage can bear is given by: $\bar{F_i} = k_i V \bar{t_i}$.

For simplicity, the average linkage survival time $\bar{t_i}$ is estimated by the most probable survival time t_i^* corresponding to the maximum of the dissociation rate(20): $d^2N/dt^2 = 0$. Therefore, $\bar{t_i}$ can be expressed as:

$$\bar{t_i} \approx t_i^* = \frac{k_B T}{k_i V l_a} \ln \left(\frac{l_a k_i V \tau_-}{k_B T} \right)$$
 [10]

The energy released upon breaking linkage i can be expressed as

$$e_i = \frac{\bar{F_i}^2}{2k_i} = \frac{V^2 \bar{t_i}^2 k_i}{2} \tag{11}$$

Substituting Eqn.10 into 11 and multiplying e_i with the number density of linkage N_i across an interface yields the energy released by advancing a unit area of an interface held by an array of slip linkages, namely, the adhesion energy:

$$G_i = \left(\frac{N}{2k_i}\right) \left(\frac{k_B T}{l_a}\right)^2 \left[\ln\left(\frac{l_a k_i V \tau_-}{k_B T}\right)\right]^2$$
 [12]

We further assume that the crack geometry remains invariant during the steady state peeling process, so $V_{\rm crack} \sim V$. We express $\tau_- = h/(k_BT) \exp{[E_i/(k_BT)]}$, where E_i and h are the activation energy of linkage i and Planck constant, respectively. To calibrate N_i , we deduced that it is limited by the area density of the chitosan chains in the bridging network $N_i \approx N_{\rm chi}$, since its size is presumably larger than that of hydrogel network and the spacing between dangling chains(14). If true, Eqn. 12 suggests that in the absence of stitch linkage, $(G/N_{chi})^{1/2}$ should only depend on $V_{\rm crack}$. Since we cannot obtain a direct measurement of N_{chi} , we adopt an approximation using the areal density of chitosan chains homogeneously dispersed in the solution using the chitosan polymer concentration $c_{\rm chi}$ (w/v%) through:

$$N_{chi} \sim \left(\frac{c_{chi}}{M_{\odot}} N_a\right)^{2/3} \tag{13}$$

Where $M_w \approx 300 \text{kDa}$, estimated from our GPC test (Fig S9) $N_a = 6 \times 10^{23}$ is the Avogadro number. Although Eqn. 13 provides a rough estimation of N_{chi} , they lead to a reasonable collapse of our data following the reformulation $(G/N_{chi})^{1/2}$ using different values of $c_{chi} = 2\%$, 1%, and 0.5% g/mL (Fig S5b and c), confirming the validity to approximate N_i by N_{chi} .

Finally, the bridging network may form slip, stitch, or the combination of the two linkages when engaging with the TEA gel, yielding the expression for the total adhesion energy(17):

$$G = \sum_{i} G_i \tag{14}$$

with

$$G_i = \left(\frac{N_i}{2k_i}\right) \left(\frac{k_B T}{l_a}\right)^2 \left[\ln\left(\frac{V_{\text{crack}} k_i l_a h}{(k_B T)^2}\right) + \frac{E_i}{k_B T}\right]^2$$

Given that an inextensible backing film was attached to the gel, V_{crack} is determined as the half of the peeling rate in the T-peel test. We then fit the model to the experimental data to estimate E_i and k_i .

Note 3: Estimation of D_{eff}

The molecular weight of a repeating unit of chitosan is approximately 160 g/mol. The averaged molecular weight of the chitosan polymer is taken to be 300 kDa (Fig. S9). The number of repeating units is thus $N \approx 1800$. We approximate that the diffusion coefficient of bridging polymers in the dangling chain layer is similar to that of bridging polymers in water, due to the extremely low polymer content in the dangling chain layer (3). According to the Rouse model, the diffusion coefficient of the polymer in water is given by

$$D_{\text{eff}} = \frac{k_B T}{N \eta b} \tag{15}$$

taking $k_BT=4.11\times 10^{-21}$ J, $N=1800,~\eta=10^{-3}$ Pa×S, b=1 nm the length of a repeating unit of chitosan, it gives $D_{\rm eff}\approx 2\times 10^{-12}~{\rm m}^2{\rm s}^{-1}$.

Note 4: Summary of topological linkages

Slip or stitch linkages.: Bridging polymer chitosan or gelatin was directly applied to gel surfaces as polymer solution. Bridging polymer chains diffuse into, and simultaneously crosslink into a network in-situ with gels with or without dangling chain layer to form slip or stitch linkages, respectively.

Bond linkage.: to form bond linkage between bridging chitosan network and tissue surfaces, we utilize the amine groups on chitosan, which can be covalently bonded to the carboxylic acid groups on tissue surfaces with EDC and NHS as coupling reagents(21): 30 mg of EDC and 30 mg of NHS were added into 1 mL of the chitosan solution for forming covalent bonds with tissue surfaces. To form the bond linkage between bridging polymers and VHB elastomer surfaces, we utilize the Carbonyl bonds on the VHB, which can form imide bonds with the amine group on the chitosan polymer at pH = 4. Besides, the ionic bond formed between NH³⁺ of chitosan of pH < 6.5 and COO⁻ of the VHB of pH > 4.5 can also contribute to the bond linkage. We prepared chitosan of pH 4.5 and hydrogel of pH 7, thus the chitosan can form an interfacial bridging network and can form both type of bonds with VHB surfaces(22).

Table S1. Types of topological linkages, their constituents (adhesive network, targeted substrate, and bridging polymer), and the associated data.

Linkage types	Adhesive network	Targeted substrate	Bridging polymer	Data
Slip-slip	TEA PAAm	TEA PAAm	Chitosan	Fig. 2d, f, Fig. S5b, c, Fig 4b,c
	~	~	Gelatin	Fig. 4b
Stitch-stitch	PAAm	PAAm	Chitosan	Fig. 2d,f
Slip-stitch	TEA PAAm	PAAm	Chitosan	Fig. 4c, Fig. S5d
Slip- bond	TEA PAAm	VHB elastomer	Chitosan	Fig. 4c
	TEA Alginate/PAAm	Porcine skin	Chitosan+EDC/NHS	Fig. 4c
	TEA Chitosan/PAAm	Porcine skin	Chitosan+EDC/NHS	Fig. 4c
Stitch- bond	PAAm	VHB elastomer	Chitosan	Fig. 4c
	Alginate/PAAm	Porcine skin	Chitosan+EDC/NHS	Fig. 4c
	Chitosan/PAAm	Porcine skin	Chitosan+EDC/NHS	Fig. 4c

Materials.

Synthesis of double network TEA. The TEA based on double-network gels was prepared with the following protocol. To prepare alginate/PAAm TEA, 1.5g alginate (I-1g) power and 6.76 g AAM were dissolved in 50 mL of deionized water. The first syringe was prepared following the aforementioned protocol, while the second syringe was added with 565 μ L of APS solution and 478 μ L calcium sulfate solution (15% w/v). The precursor solutions were quickly syringe-mixed and immediately poured into 80 \times 20 \times 3 mm³ rectangular acrylic molds covered with PMMA on the two sides, and then kept at room temperature for 24 hours to complete the reaction. To prepare the chitosan/PAAm TEA, acrylamide and chitosan powders were first dissolved in 0.2 M acetic acid at 3.3 mol/L and 2.5%, respectively. MBAA was then added to the AAm-chitosan solution at 0.0006:1 the weight of acrylamide to complete the polymer precursor solution. To prepare a gelling solution to crosslink the chitosan, 0.1 M Na₂HPO₄ and 0.1 M NaH₂PO₄ were first mixed with a volume ratio of 50:3. Sodium bicarbonate was then added to the solution at a concentration of 0.306 M. A mass fraction of 6.6% APS was later added to the solution as an initiator. Both solutions were degassed, quickly mixed at 3:2 volume ratio (polymer precursor to gelling solution) using syringes and injected into a mold with substrates of choice for overnight gelation. To prepare the regular alginate/PAAm and PAAm chitosan gels, we follow the same procedure except for injecting the mixed solution into the acrylic molds covered by glass sheets on the two sides followed by the gelation process.

Methods.

Adhesion test. The TEA gels were prepared with a length of 80 mm (or 40 mm), width of 20 mm, and thickness of 3 mm, or otherwise specified. To test their adhesion on gels and VHB elastomers, the surface of TEA was treated with the bridging polymer solution of $0.25~\mu\text{L/mm}^2$, and then immediately covered with the adherend. An instant compression of 15% strain was applied to remove the excessive solution on the interface. No prolonged compression was applied. For testing TEA adhesion on tissue samples, bridging polymer solution with chemical reagents added was applied to the tissue surface, followed by covering with the TEA gel. A continuous compression of 15% strain, or otherwise specified, over the whole course of adhesion establishment was applied to the TEA-tissue sample. To measure the adhesion energy, standard T-peeling(180-degree peeling) was performed. The tests were conducted using a universal testing machine (Instron Model 5365) with 10N and 1kN load cells. Before test, PET backing is attached to the samples using Krazy glue. In a typical test, the peeling force reaches a plateau F_{plateau} once reaching the steady state process (Fig S5a). The adhesion energy is calculated as twice the plateau force divided by the sample width, $G = 2F_{\text{plateau}}/w$. The loading rate was varied from 0.2 mm/s to 40 mm/s. Given the rigid backing, the crack speed for 180-degree peeling is half the loading rate.

Adhesion kinetics test. To characterize adhesion kinetics, nylon mesh of different thicknesses (50 and 120 μm) were used to define the thickness of the bridging polymer solution h_{sol} following a previously reported protocol(23). We first immersed the nylon mesh in the bridging polymer solution, and then removed the excessive solution on the surface before applying it to the interface between two pieces of hydrogels. We waited for different time t before measuring adhesion energy using T-peeling test at a relative low crack speed $V_{\text{crack}} = 0.5 \text{ mm/s}$. The adhesion energy increases with t and reaches the equilibrium value G_{eq} . The adhesion energy versus waiting time was fitted by the function $G = G_{eq}(1 - e^{t/t_{1/2}})$, where the half time $t_{1/2}$ can be extracted as the fitting parameter.

Uniaxial tensile test. Samples with length of 40mm, width of 20mm, thickness of 3mm were prepared and tested using the Instron machine with 1N and 1kN load cells. The nominal stress is calculated using $\sigma = F/A$ where F and A are the measured 211 force and cross-sectional area of the sample. The stretch is calculated as $\lambda = \lambda_1/\lambda_0$ where λ_1 is the current length and λ_0 is 212 the initial length. 213

Micro-indentation test. The set-up utilizes an XYZ linear stage (Optosigma, Santa Ana, CA) with a range of \pm 6.5 mm for the 214 X and Y directions and \pm 5 mm for the Z direction. The resolution for all three directions is 10μ m (Fig S2a). An aluminum 215 beam was mounted to the XYZ stage, with its other end connected to a load cell (Interface Inc., Scottsdale, AZ) with a capacity 216 of 1 N and a resolution of 100 μ N. We use a rigid spherical indenter (i.e., a steel ball) with a radius of ≈ 1.25 mm. 217

Finite element (FE) modelling. We performed FE modelling to estimate the modulus of the dangling chain layer when it is 218 under compression using a commercially available package ABAQUS 2019. In the model, the spherical indenter is modelled as 219 a rigid body, and is subjected to a prescribed displacement loading condition. The "dangling chain region" and the "bulk 220 network" are modelled using linear elastic model with elastic moduli $E_{\rm dc}$ and $E_{\rm bulk}$, and with axisymmetric solid elements 221 (CAX). Standard/static solver was used to simulate the indentation process.

Atomic force microscopy (AFM). An atomic force microscope (JPK NanoWizard@3, Berlin, Germany) was used to conduct 223 nano-indentation tests. Rectangular silicon cantilevers with 0.6 μm -in-diameter spherical beads attached as probes were used 224 (Novascan, IA, USA). Cantilevers with a nominal spring constant of 0.6 N/m were used for experiment. The cantilever spring constants were determined using thermal noise method before the experiment. Hydrogel samples were immersed in PBS for 3 hours before indentation to avoid fast swelling during test. Then swollen hydrogels were glued to 35-mm Petri dishes and 227 immersed in PBS during the measurement. Hertzian contact model was used to fit the indentation data and to calculate the 228 Young's modulus. 229

Scanning electron microscope (SEM). The structures of hydrogels were imaged using a field emission scanning electron 230 microscope (FE450, FEI) under various magnifications. Before SEM imaging, all the samples were immersed in sucrose solution 231 (20% w/v) over night, cryo-sectioned, and dehydrated in open air. The dehydrated samples were coated 4 nm Pt using a 232 high-resolution sputter coater (ACE600, Leica) to increase surface conductivity. A conductive tape was used to mount the 233 sample to the imaging platform. 234

GPC test. Chitosan samples with a concentration of 1 mg/mL were dissolved in an aqueous acetate buffer (0.25 M acetic acid, 0.25 M Na acetate) overnight, with stirring. They were filtrated (0.45 μ m) prior to be transferred to the autosampler vials. 100 µL injection was analyzed using a SEC column OHpak SB-805 HQ (8 mm ID x 300 mm L) at a flow rate of 0.3 mL /min of the eluting phase (same as the one in which samples were dissolved). The signal of the RI detector was used for calculation of the molecular weights and PDI against a calibration curved constructed with pullulan standards of narrow polydispersity and molecular weight in the 5.9 to 788 kDa range.

Confocal microscopy. Hydrogel samples with diffused bridging polymers were imaged with a confocal microscope (LSM 710, Zeiss). Hydrogel samples with diffused FITC-chitosan were cut into thin slices by a blade and transferred to a 35 mm Petri dish with coverslip bottom (MatTek, P35G-0-10-C). The polymer network was imaged with 10X and 20X objective lenses. 243 Axiovert A1 inverted microscope (Zeiss) equipped with a motorized stage was used to obtain fluorescent signals at multiple locations. Light intensity was maintained the same for all the samples. 245

Patterned TEA. A PTFE tape of thickness 0.1mm was designed into different shapes and then adhered to a glass plate (Fig S7e left). Alternatively, four glass slides of thickness 1mm and a PTFE sheet of thickness 0.9 mm was assembled in the plane (SI 247 Appendix Fig S7e right). A rectangular acrylic mold was placed on top of patterned substrate. After injecting pre-gel solution, 248 the mold was covered with another glass plate. The two approaches result in different flatnesses of the gel surface but both 249 yielding high-fidelity adhesion selectivity.

TEA-based wound patch. A PTFE tape of thickness 0.1mm was designed into a circle of diameter 1.5 cm, and then adhered to a glass plate. A rectangular acrylic mold was placed on top of patterned substrate. After injecting pre-gel solution, the mold was covered with another glass plate. Biopsy punch was used to generate circular wounds on rat skin (diameter of 6mm) and porcine stomach (diameter of 1cm). When de-molded, the TEA gel was applied to wounds on rat skin and porcine stomach with 2% chitosan and EDC/NHS reagents. A prolonged compression for 3 mins was then applied by hand. The size of the circular danlging chain region of the TEA adhesive can be tailored to suit different sizes of the wounds.

203

204

205

207

209

235

236

237

238

244

251

TEA-based fluidic channels. A PTFE tape of rectangular (or 'S'-shape) was attached to a glass plate. Pre-gel solution is injected into the mold for reaction to complete. Once de-molded, we use hole punch of diameter 2 mm to create an inlet hole and an outlet hole, and then attach it to a targeted surface using chitosan as bridging polymer. If the targeted surface is tissue, we also added chemical reagents to form covalent bonds between chitosan and tissue surfaces. After the adhesion is established, we further insert two soft tubes into the inlet and outlet, sealed using Crazy glue, and slowly inject liquid to cleave the weak adhesion by slip linkages. The fluidic channel is formed once the whole weak interface is separated.

TEA-based Drug eluting devices. A SN PAAm TEA gel was first prepared on a glass mold substrate patterned with a circular PTFE film of diameter 2 cm. It was then adhered to a regular gel which was glued onto an acrylic sheet. The circular low-adhesion region served as local depot to which drugs will be injected. The albumin-FITC (A9771, Sigma-Aldrich) was used as a model drug and was dissolved in PBS at 10 mg/mL to get the drug solution. At equilibrium of hydrogels, different volume of drug solution (0.2 mL and 0.5 mL) was slowly injected into the weak interface, resulting in local drug punches inside the hydrogel. After the injection, the whole device was immersed in 200 mL PBS. At determined time points, the fluorescence intensity of the solutions was measured using a BioTek Synergy HTX multi-mode microplate reader (λ ex = 485/20 nm, λ em = 528/20 nm). A standard calibration curve was made in order to calculate the concentration of released drug.

TEA-based reconfigurable soft actuators. Individual actuator module was prepared using a molding process. SN PAAm pregel solution was injected to a 3D printed mold made of PLA (Fig S8). The mold was then covered by a PMMA sheet. Once the reaction is completed and demolded, the actuator module readily carries dangling chains on its surface. Different modules were connected by applying bridging polymer chitosan to the interface. To separate the connected modules, a small force with a low separate rate can be applied. The separated modules can be reconnected following reapplying bridging polymers to the interface.

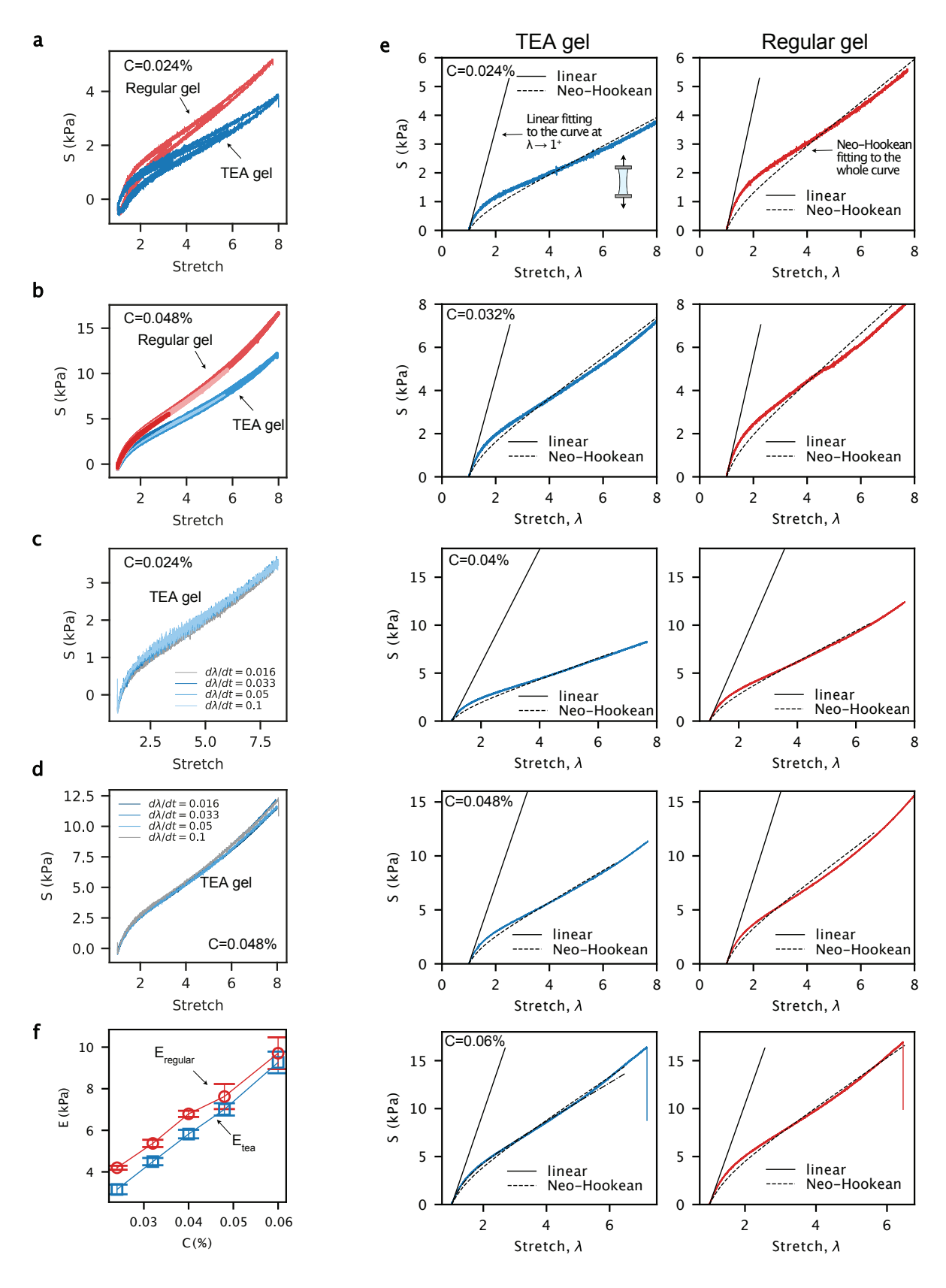


Fig. S1. (a) Uniaxial cyclic tensile tests of a TEA and a regular gel made of SN PAAm for C=0.024%. (b) the same curves as (a) for C=0.048%. Uniaxial tensile test results of SN TEA gels with varying strain rates for (c) C=0.024% and (d) C=0.048%. (e) representative stress-stretch curves of TEA (left) and regular (right) gels for different values of C measured in uniaxial tensile tests. (f) Measured elastic moduli by the linear model for SN TEA and regular gels, plotted as functions of C.

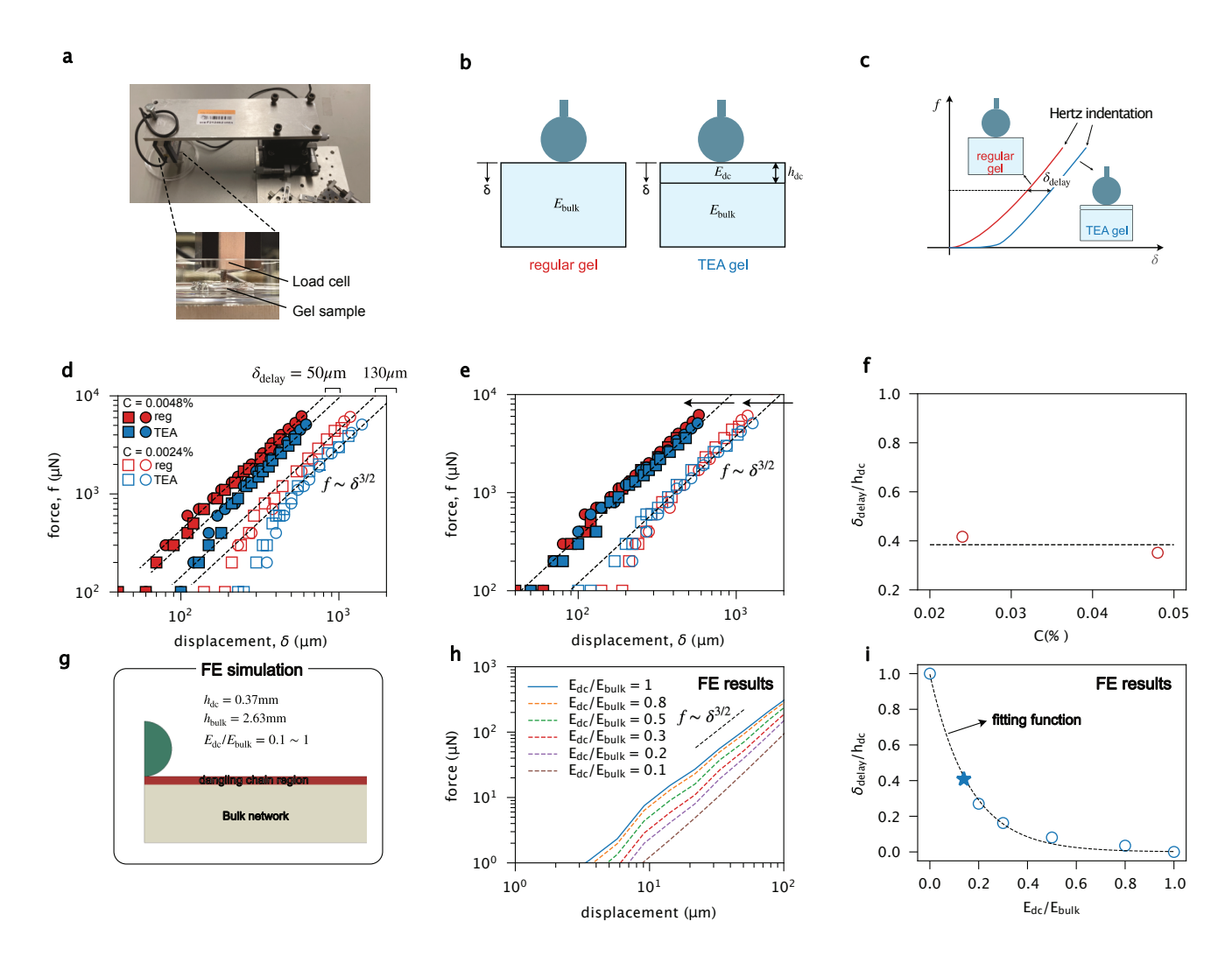


Fig. S2. Micro indentation test of TEA and regular gels. (a) Experimental set up. (b) Schematics showing indentation test on regular and TEA gels. (c) Schematics showing the proposed indentation behavior on the two types of gels. (d) Indentation results on regular and TEA gels, with two different C values. (e) Same as in (d) but with the curves of TEA gels shifted by their respective $\delta_{\rm delay}$ values. (f) Ratio $\delta_{\rm delay}/h_{\rm dc}$ calculated using data in (d) and in Fig 2c, as a function of C. (g) Schematic illustrating the FE modeling of the indentation test. (h) force-displacement curves extracted from the FE simulation, for different $E_{\rm dc}/E_{\rm bulk}$ values. (i) $\delta_{\rm delay}/h_{\rm dc}$ plotted as a function of $E_{\rm dc}/E_{\rm bulk}$ extracted from the FE simulation.

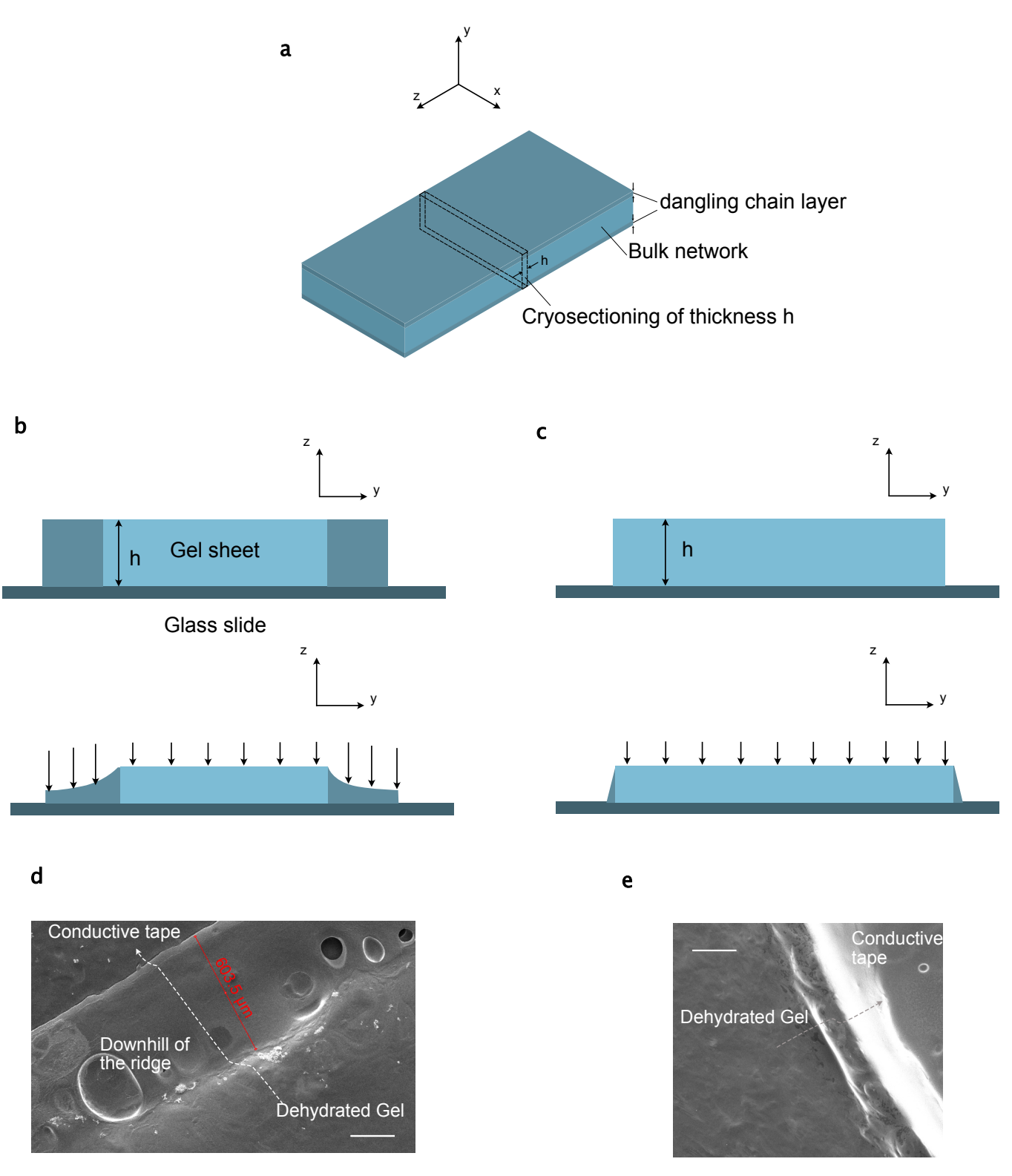


Fig. S3. Cryosectioning of TEA and regular gels with C=0.024%. (a) Schematic showing the dimension of the samples. The samples were prepared by first immersing them in sucrose solution overnight, followed by immersing them in OCT solution overnight. The samples were then cryosectioned into sheets of thickness $h=100\mu\mathrm{m}$, transferred to glass slides, and dehydrated in open air. (b) Schematic showing the cross-sectional sheet of the cryosectioned TEA gel in the wet (top) and dehydrated (bottom) conditions. The sheet shrinks more significantly near the edge than in the center. (d) SEM image of a cryosectioned and dehydrated TEA gel sheet. They show "ridges" near the edge due to the inhomogeneous shrinkage. (c) Schematic showing the cross-sectional sheet of a cryosectioned and dehydrated regular gel in the wet (top) and dehydrated (bottom) conditions. (e) SEM image of a dehydrated regular gel sheet, showing less edge shrinkage effects. Scale bars in (d) and (e) are $200\mu\mathrm{m}$.

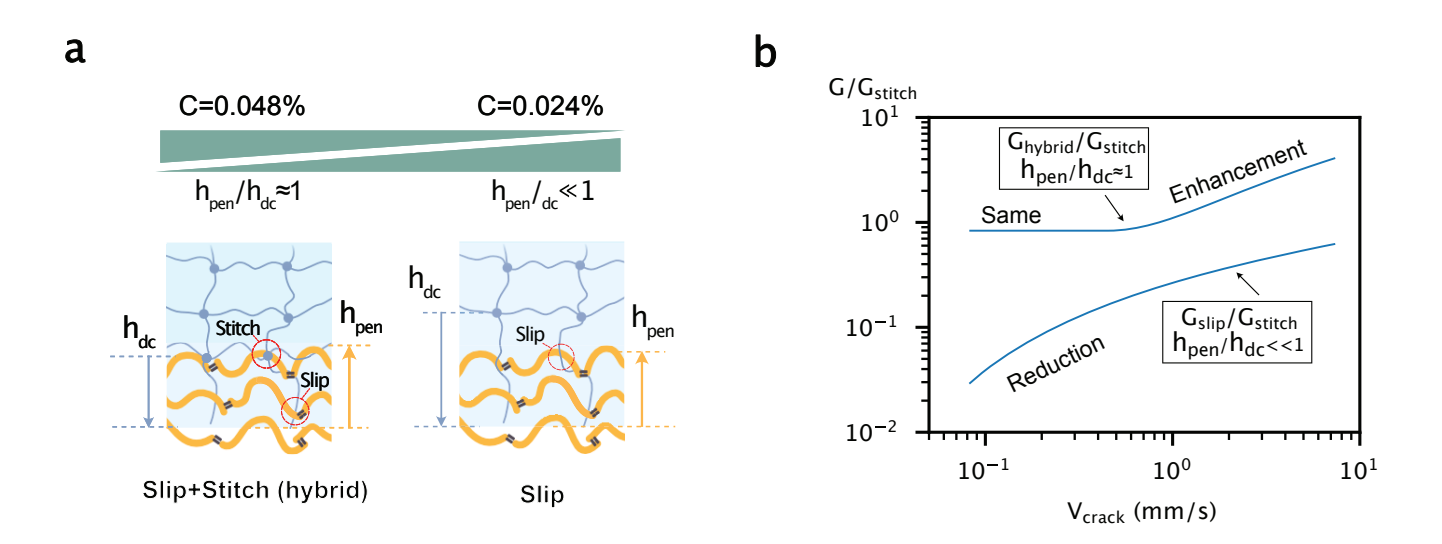


Fig. S4. (a) Illustrations showing the effects of entanglement length on the formation of slip and stitch linkages. (b) Adhesion contrast between the slip and stitch regions in a patterned TEA for given C and $h_{\rm pen}/h_{\rm dc}$ values. The slip linkage becomes the hybrid linkage as $h_{\rm pen}/h_{\rm dc}$ becomes closer to 1.

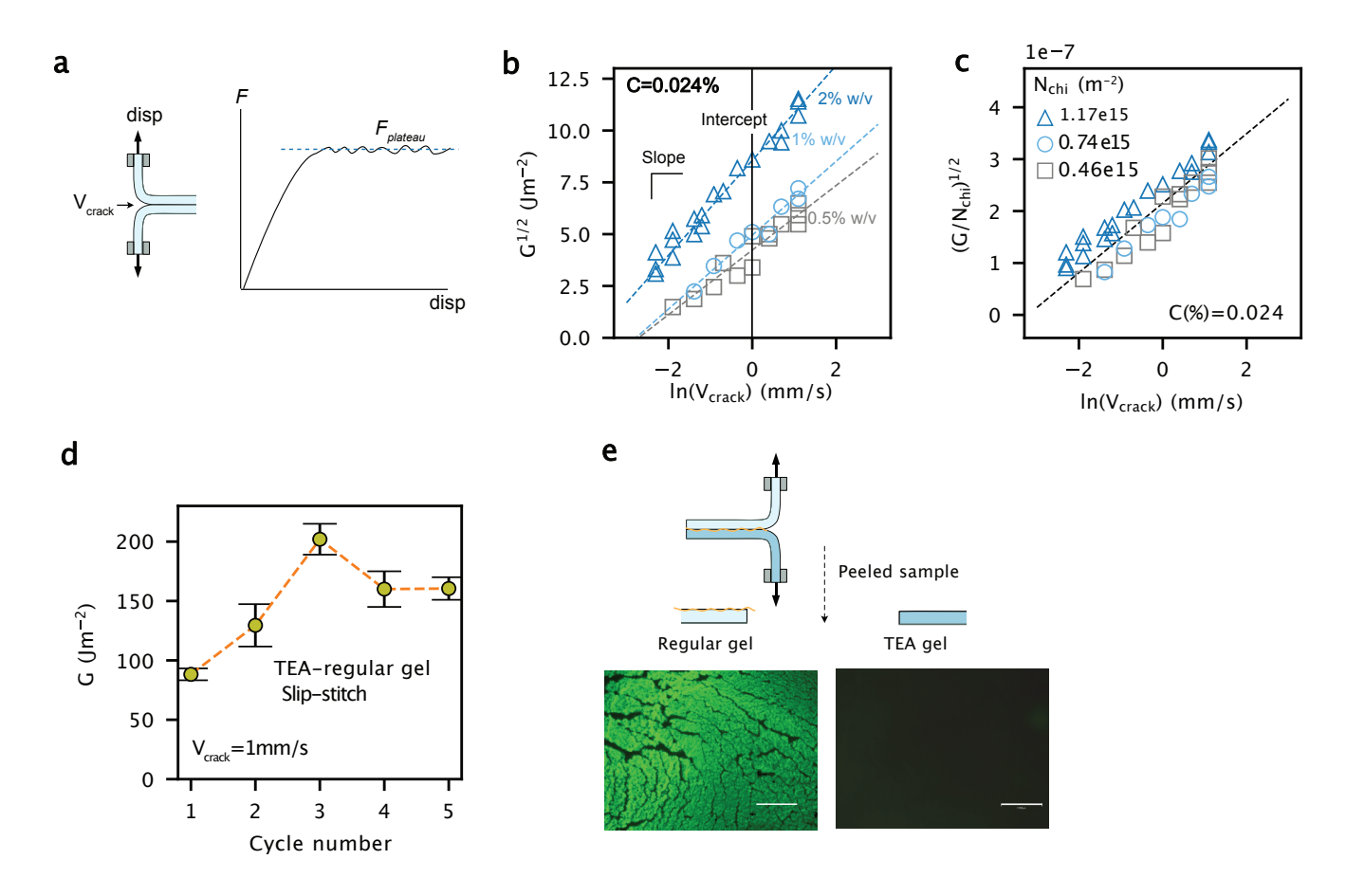


Fig. S5. Schematic showing the T-peeling test and the resulting force-displacement curves. The adhesion energy is interpret as $G=2F_{plateau}/w$, with w the out-of-plane thickness of the sample. (b) $G^{1/2}$ by the slip-slip linkage plotted as a function of $\ln V_{\rm crack}$ for C=0.024% and varying c_{chi} (0.5%, 1%, and 2% g/mL) (c) reformulated $(G/N_{chi})^{1/2}$) for C=0.024%, where N_{chi} is estimated using Eqn 13. (d) Cyclic peeling test on a TEA-regular interface at $V_{\rm crack}$ =1mm/s. After every peeling, a new regular gel adheres to the same TEA gel with newly applied chitosan solution. The adhesion increases and stabilizes after 5 cycles. (e) Peeled regular gel and TEA gel after a peeling test. The interface was bonded with a slip-stitch linkage using fluorescently labeled chitosan. After peeling, the chitosan network remains on the regular gel, but remains minimally in the TEA gel. Scale bars: 1mm.

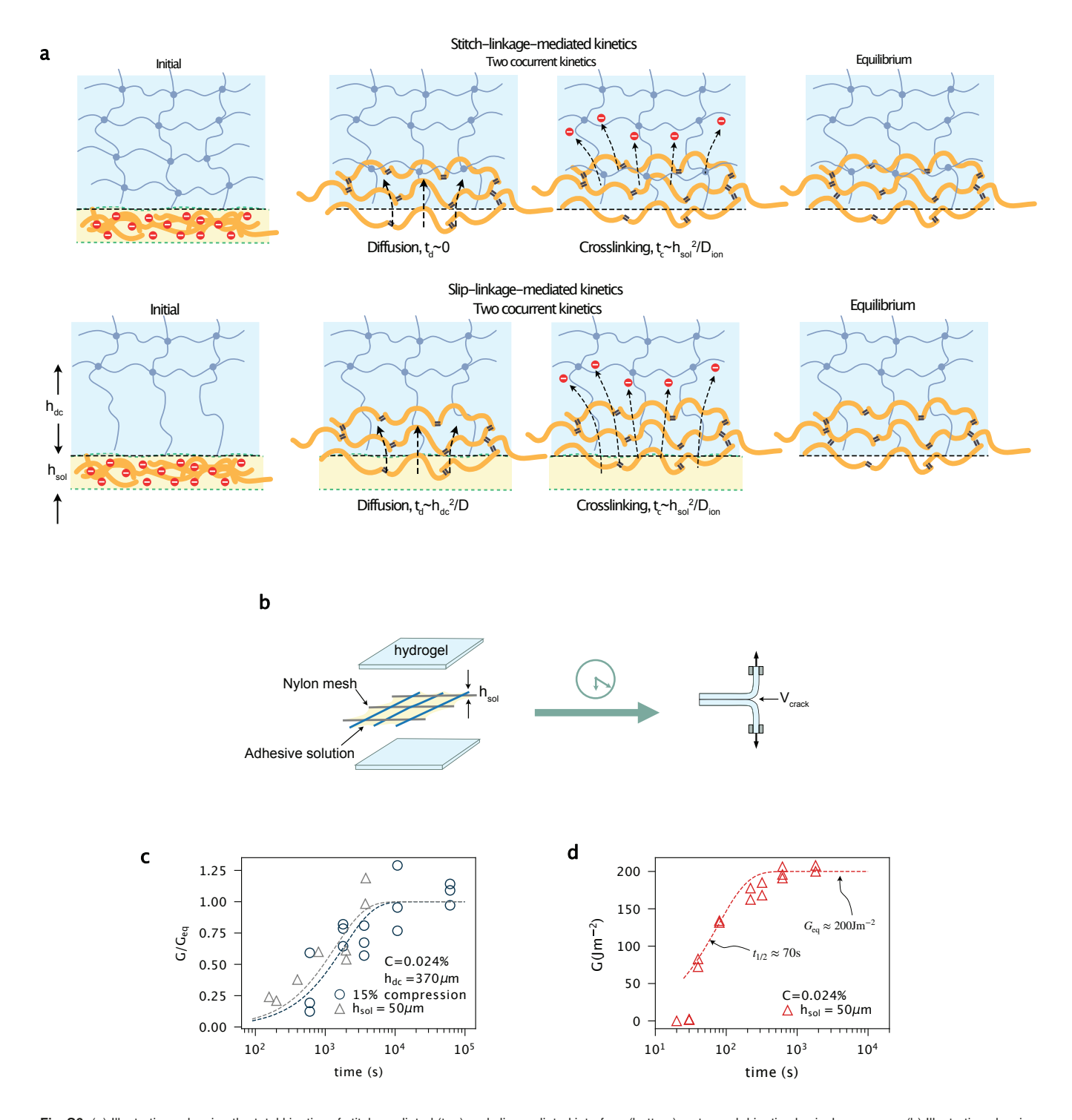


Fig. S6. (a) Illustrations showing the total kinetics of stitch-mediated (top) and slip-mediated interface (bottom) as two sub kinetic physical processes. (b) Illustration showing the experimental procedure to characterize the adhesion kinetics of TA and TEA. (c) Dimensionless adhesion $G/G_{\rm eq}$ as functions of waiting time for TEA with $h_{\rm dc}=370\mu m$. In one case $h_{\rm so1}=50\mu m$ was controlled by using nylon mesh of the same thickness at the interface. In the other case, an initial compression strain of 15% was applied to the sample after applying adhesive solution without using the thickness-defining mesh, such that $h_{\rm so1}$ was not well-controlled. No prolonged compression was applied. (d) Adhesion energy G between two regular hydrogels with G=0.024% as a function of waiting time for cast solution thicknesses $h_{\rm so1}=50\mu m$. $G_{\rm eq}\approx200{\rm Jm}^{-2}$ and $t_{1/2}\approx70{\rm s}$.

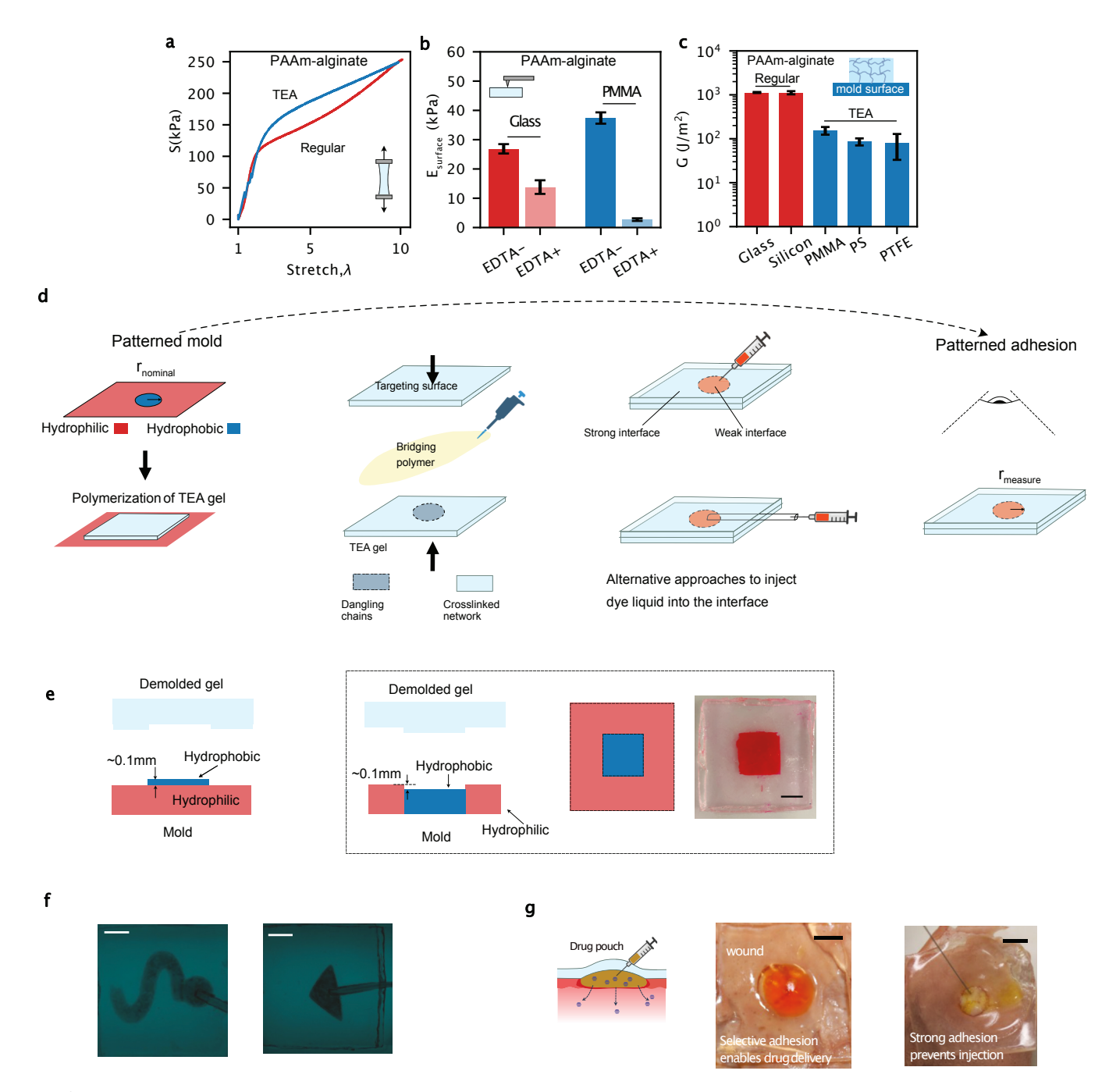


Fig. S7. (a) Uniaxial tensile test results show similar engineering stress-stretch curves for a DN TEA and a DN regular alginate/PAAm gels. (b) AFM test on the surface of the DN gels polymerized on PMMa and glass molds with and without EDTA treatment, which can disassociate the ionic crosslinker in the alginate network. For DN gels made on PMMa mold, the difference in the surface moduli with and without EDTA treatment is more pronounced than those made on glass mold, suggesting the presence of surface dangling chains in the DN gels made on PMMa molds. (c) Adhesion of alginate/PAAm gels made on different mold surfaces on porcine skin. In this study, the continuous compression strain applied to these samples during the course of adhesion establishment is ~ 30%, and the dimension of the samples is 80mm(length)×15mm(width)×1.5mm(thickness). The applied crack speed is 0.25mm/s. (d) Schematic illustrating the procedure for creating spatially programmable adhesion of TEA: a needle is used to penetrate the hydrogel into the interface, or a tube was sandwiched between the two gels. Next, liquid dye was injected through the needle or the tube. Finally, a digital camera was used to capture the weak interface through the liquid dye. (e) Illustration of the two strategies to pattern the surface of the gels. Left and right strategies result in a dent and a bump on the demolded gel surface where dangling chain forms, respectively. The strategy shown in left produces high fidelity selective adhesion in Fig S5(f) and Fig 5, while the strategy shown in right also results in high fidelity selective adhesion, shown in the box. Scale bar: 1cm. The results prove that the flatness of the gels does not affect the designed adhesion selectivity. (f) Patterned interface formed between a TEA alginate/PAAm gel and a regular alginate/PAAm gel. The TEA gel is designed with designed dangling chain regions of different shapes, resulting in weak interfaces of the identical shape. Scale bar: 10 mm. (g) Mock drug is injected to the wounded porcin

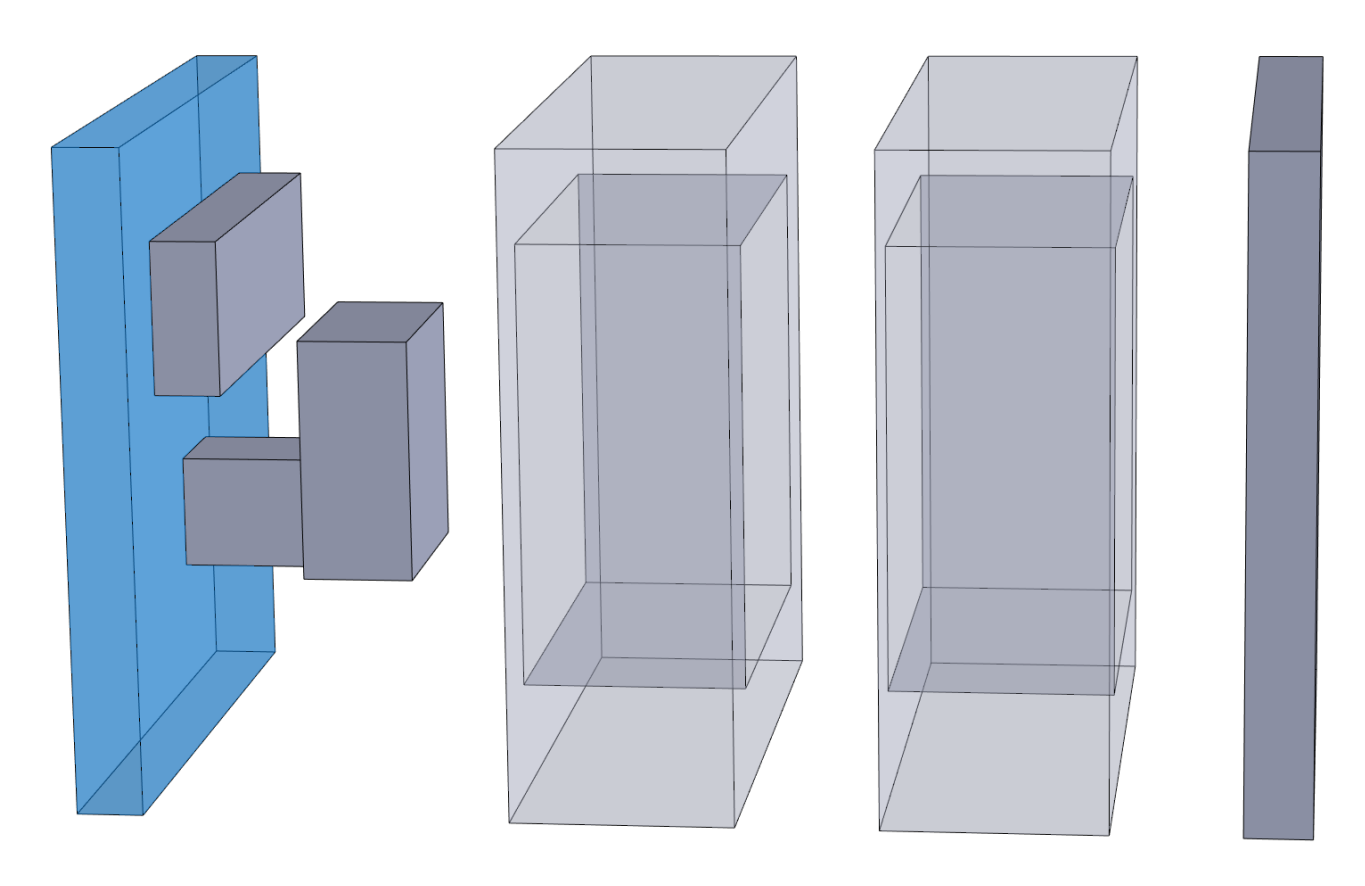


Fig. S8. 3D printed mold for creating soft actuator modules. The mold parts are 3D-printed using PLA. The cover, indicated in blue, is made of PMMA.

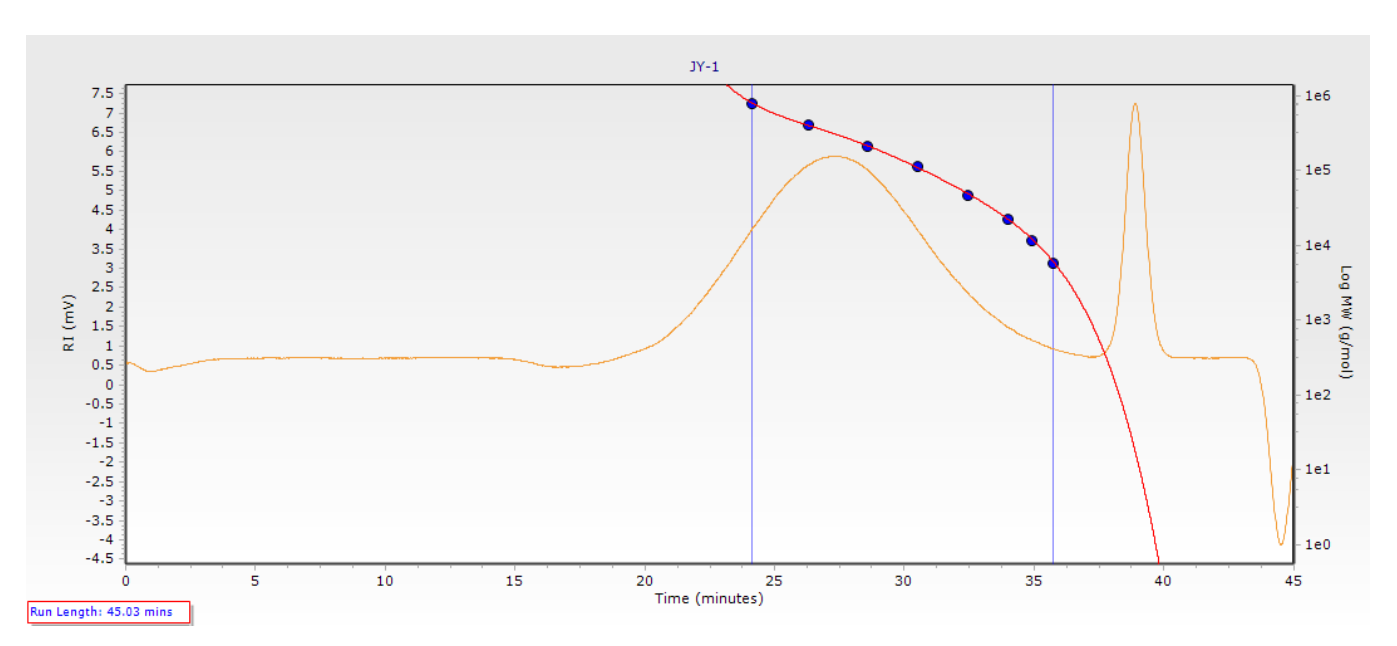


Fig. S9. GPC test results. An approximated value of molecular weight may be calculate using the equation of the calibration curve: $y=-3.306E-05x^5+0.004911x^4-0.2913x^3+8.624x^2-127.4x+757.8$ Where x is equal to the elution time (27.42 min). (MW is between 212 and 404 kDa. An approximated value $MW \approx 300$ kDa is used in calibration the area density of slip and stitch linkage in *SI Appendix* Note 2.)

278

279

280

281

285

286

287

288

289

290

291

292

293

294

295

296

297

299

300

301

302

303

304

307

308

312

References

- 1. JP Gong, A Kii, J Xu, Y Hattori, Y Osada, A possible mechanism for the substrate effect on hydrogel formation. *The J. Phys. Chem. B* **105**, 4572–4576 (2001).
- 2. A Kii, J Xu, JP Gong, Y Osada, X Zhang, Heterogeneous polymerization of hydrogels on hydrophobic substrate. *The J. Phys. Chem. B* **105**, 4565–4571 (2001).
- 3. JP Gong, et al., Synthesis of hydrogels with extremely low surface friction. J. Am. Chem. Soc. 123, 5582–5583 (2001).
- 4. J Mandal, K Zhang, ND Spencer, , et al., Oxygen inhibition of free-radical polymerization is the dominant mechanism behind the "mold effect" on hydrogels. *Soft Matter* 17, 6394–6403 (2021).
- 5. K Zhang, R Simic, W Yan, ND Spencer, Creating an interface: rendering a double-network hydrogel lubricious via spontaneous delamination. ACS Appl. Mater. & Interfaces 11, 25427–25435 (2019).
- 6. W Hong, Z Liu, Z Suo, Inhomogeneous swelling of a gel in equilibrium with a solvent and mechanical load. *Int. J. Solids Struct.* **46**, 3282–3289 (2009).
- 7. A Chau, M Cavanaugh, YT Chen, A Pitenis, A simple contact mechanics model for highly strained aqueous surface gels. *Exp. Mech.* **61**, 699–703 (2021).
- 8. T Narita, et al., Microrheological investigation of substrate-induced gradient structure in hydrogels. *Macromolecules* **34**, 5725–5726 (2001).
- 9. Y Yu, D Sanchez, N Lu, Work of adhesion/separation between soft elastomers of different mixing ratios. *J. Mater. Res.* **30**, 2702–2712 (2015).
- RW Style, A Jagota, CY Hui, ER Dufresne, Elastocapillarity: Surface tension and the mechanics of soft solids. Annu. Rev. Condens. Matter Phys. 8, 99-118 (2017).
- 11. M Manay, M Ponga, AS Phani, Stress in a polymer brush. J. Mech. Phys. Solids 127, 125–150 (2019).
- 12. I Argatov, FM Borodich, X Jin, Atomic force microscopy of polymer brushes: insights into controversies. Front. Mech. Eng. 8, 931271 (2022).
- 13. CH Mathis, et al., Indenting polymer brushes of varying grafting density in a viscous fluid: A gradient approach to understanding fluid confinement. *Polymer* **169**, 115–123 (2019).
- 14. J Yang, R Bai, Z Suo, Topological adhesion of wet materials. Adv. Mater. 30, 1800671 (2018).
- 15. HR Brown, Effects of chain pull-out on adhesion of elastomers. Macromolecules 26, 1666-1670 (1993).
- ³⁰⁵ 16. GI Bell, Models for the specific adhesion of cells to cells: a theoretical framework for adhesion mediated by reversible bonds between cell surface molecules. *Science* **200**, 618–627 (1978).
 - 17. MK Chaudhury, Rate-dependent fracture at adhesive interface. The J. Phys. Chem. B 103, 6562–6566 (1999).
 - 18. IV Pobelov, et al., Dynamic breaking of a single gold bond. Nat. communications 8, 15931 (2017).
- 19. CY Hui, T Tang, YY Lin, MK Chaudhury, Failure of elastomeric polymers due to rate dependent bond rupture. *Langmuir* **20**, 6052–6064 (2004).
- 20. E Evans, K Ritchie, Dynamic strength of molecular adhesion bonds. Biophys. J. 72, 1541–1555 (1997).
 - 21. J Li, et al., Tough adhesives for diverse wet surfaces. Science 357, 378–381 (2017).
- 22. J Yang, et al., Design molecular topology for wet-dry adhesion. ACS Appl. Mater. & Interfaces 11, 24802–24811 (2019).
- 23. J Steck, J Kim, J Yang, S Hassan, Z Suo, Topological adhesion. i. rapid and strong topohesives. *Extrem. Mech. Lett.* **39**, 100803 (2020).